MICROCOPY RESOLUTION TEST CHART

NATIONAL BUREAU OF STANDARDS-1963-A

Wind-Tunnel Evaluation of an Advanced Main-Rotor Blade Design for a Utility-Class Helicopter

DTIC
S ELECTE D
SEP 1 7 1987

William T. Yeager, Jr., Wayne R. Mantay,
Matthew L. Wilbur, Robert G. Cramer, Jr.,
and Jeffrey D. Singleton

SEPTEMBER 1987

NASA

US ARMY
AVIATION
SYSTEMS COMMAND
AVIATION R&T ACTIVITY

87   9 16 090

Wind-Tunnel Evaluation of an Advanced Main-Rotor Blade Design for a Utility-Class Helicopter

William T. Yeager, Jr., Wayne R. Mantay,
Matthew L. Wilbur, Robert G. Cramer, Jr.,
and Jeffrey D. Singleton

Aerostructures Directorate
USAARTA-AVSCOM
Langley Research Center
Hampton, Virginia

Accesion For		
NTIS CRA&I	☑	
DTIC TAB	☐	
Unannounced	☐	
Justification		
By		
Distribution /		
Availability Codes		
Dist	Avail and / or Special	
A-1		

QUALITY INSPECTED 2

Summary

An investigation was conducted in the Langley Transonic Dynamics Tunnel to evaluate differences between an existing utility-class main-rotor blade and an advanced-design main-rotor blade. The two rotor-blade designs were compared with regard to rotor performance, oscillatory pitch-link loads, and 4-per-rev vertical fixed-system loads. Tests were conducted in hover and over a range of simulated full-scale gross weights and density altitude conditions at advance ratios from 0.15 to 0.40. Results indicate that the advanced-blade design offers performance improvements over the baseline blade in both hover and forward flight. Pitch-link oscillatory loads for the baseline rotor were more sensitive to the test condition than those of the advanced rotor. The 4-per-rev vertical fixed-system load produced by the advanced blade was larger than that produced by the baseline blade at all test conditions.

Introduction

Historically, the helicopter industry has not relied on wind-tunnel testing of scaled models to the same degree as the fixed-wing industry (ref. 1). The reason for this lack of testing has been that new rotor designs have usually evolved from existing designs. The new rotor designs had aeroelastic and aerodynamic characteristics that could be reasonably predicted by extrapolating existing data; thus, the need for wind-tunnel testing was reduced. Changes in rotorcraft mission requirements and technology have led to the development of new rotor systems, incorporating hingeless and bearingless hub designs as well as main-rotor blades with unique planform and twist geometries and with new families of airfoils, and incorporating passive means of reducing fixed-system vibration levels. These unique main-rotor system designs have provided the impetus to address the problems of rotor system loads, stability, vibration characteristics, and overall performance during the design phase through the combined use of analysis and proof of concept testing, rather than providing "fixes" to problems as they occur during development. Recent examples of the use of analysis and testing during the design phase are discussed in references 2 and 3.

An effort that combines analysis and testing has been used to design and evaluate an advanced main-rotor blade for the U.S. Army's UH-60A Black Hawk helicopter. The blade aerodynamic characteristics (airfoil selection, planform, twist, and solidity) were analytically designed for hover and forward flight using the approach described in reference 4. Reference 4 uses a hover analysis which combines the momentum theory and the blade-element theory (ref. 5),

and forward-flight analysis makes use of the computer program described in reference 6. The advanced rotor was designed to provide performance improvements, in terms of rotor torque requirements, over the present UH-60A rotor in both hover and forward flight. Of particular interest are conditions involving increases in the present UH-60A mission gross weights and parasite drag requirements (e.g., external cargo at sea-level conditions and at increased-density-altitude atmospheric conditions). The present UH-60A rotor was not designed to meet these increased mission requirements.

The evaluation of the advanced-rotor blade design was conducted in the Langley Transonic Dynamics Tunnel in a Freon 12 [1] atmosphere using 1/6-size models of the advanced-design rotor blades and baseline UH-60A rotor blades. The baseline blades were included to provide a measure of the gross differences in performance and loads between the two configurations. Testing was conducted in hover and forward flight up to an advance ratio of 0.40. In addition to evaluating the advanced-blade aerodynamics and loads, the model advanced blades were designed to allow the addition of nonstructural mass to the blades to evaluate blade modal shaping (ref. 7) for reducing fixed-system vibratory loads. The discussion presented in this report is intended to provide an overview of the data obtained.

Symbols

The positive directions of forces, angles, and velocities are shown in figure 1.

A	balance axial force, lb
a	speed of sound, ft/sec
C_D	rotor drag coefficient, $\dfrac{D}{\rho \pi R^2 (\Omega R)^2}$
C_L	rotor lift coefficient, $\dfrac{L}{\rho \pi R^2 (\Omega R)^2}$
$C_{L,max}$	rotor-blade section maximum lift coefficient
C_Q	rotor torque coefficient, $\dfrac{Q}{\rho \pi R^3 (\Omega R)^2}$
D	rotor drag, lb, $N \sin \alpha_s + A \cos \alpha_s$
d	rotor diameter, ft
FSO_{4p}	normalized 4-per-rev vertical fixed-system (balance normal force) load

f_D	vehicle equivalent parasite area, ft^2
I_θ	rotor-blade torsional mass moment of inertia per foot about blade elastic axis, lb-sec^2
L	rotor lift, lb, $N\cos\alpha_s - A\sin\alpha_s$
M_T	rotor hover tip Mach number, $\frac{\Omega R}{a}$
N	balance normal force, lb
PL	normalized pitch-link oscillatory load
Q	rotor-shaft torque, measured from balance yawing-moment channel, ft-lb
R	rotor radius, ft
r	spanwise distance along blade radius measured from center of rotation, ft
SL	sea-level atmospheric density conditions
SLS	sea-level atmospheric density conditions at 59°F
V	free-stream velocity, ft/sec
z	distance from wind-tunnel floor to rotor hub, ft
α_s	rotor-shaft angle of attack, deg
θ	rotor-blade collective pitch angle at $\frac{r}{R} = 0.75$, deg
θ_1	twist angle built into rotor blade, positive nose up, deg
μ	rotor advance ratio, $\frac{V}{\Omega R}$
ρ	mass density of test medium, slugs/ft^3
ψ	rotor-blade azimuth angle, deg
Ω	rotor rotational velocity, rad/sec
ω	natural frequency of rotating-blade mode, rad/sec

Apparatus and Procedures

Wind Tunnel

The testing was conducted in the Langley Transonic Dynamics Tunnel (TDT). A schematic of the tunnel is shown in figure 2. The TDT is a continuous-flow tunnel with a slotted test section and is capable of operation up to Mach 1.2 at stagnation pressures up to 1 atm. The tunnel test section is 16 ft square with cropped corners and has a cross-sectional area of 248 ft^2. Either air or Freon 12 may be used as a test medium. For this investigation, Freon 12 at a nominal density of 0.006 slug/ft^3 was used as the test medium. Because of its high density and low speed of sound, the use of Freon 12 aids the matching of model-rotor-scale Reynolds number and Mach number to full-scale values. Since the primary purpose of these tests involved rotor performance, matching full-scale Mach number at Reynolds numbers higher than those obtainable by testing in air was of particular interest. The use of Freon 12 as a test medium also allows the easing of some restrictions on model structural design while still maintaining dynamic similarity. For example, a heavier test medium permits a simplified structural design to obtain the required stiffness characteristics, and thus eases design and fabrication requirements of the model (ref. 8).

Model Description

The model rotor hub used in this investigation was a four-bladed articulated hub with coincident lead-lag and flapping hinges. The hub operated with a measured pitch-flap coupling ratio of 0.5 (flap up, pitch down). The location of the pitch-link attachment point is shown in figure 3. Two sets of blades were used during these tests: a set of baseline UH-60A blades and a set of advanced-design blades. The planform geometry and twist distribution of each set of blades are shown in figures 3 and 4, respectively. The structural properties and rotating natural frequencies of each blade set are presented in tables I and II. The rotating natural frequencies were calculated using the CAMRAD analysis described in references 9 and 10.

The baseline blades were a 1/6-size, Mach scaled representation of UH-60A rotor blades. The model-scale baseline blade structural properties (table I) were established by scaling full-scale blade properties, although no attempt was made to exactly match the distributions of the full-scale blades (ref. 11). The baseline blades used SC1095 and SC1095-R8 airfoils. The aerodynamic characteristics of these two airfoils are documented in reference 12. The area, thrust-weighted, and torque-weighted solidities for the baseline rotor were 0.0825. Figure 3 shows that the baseline blades were equipped with adjustable trailing-edge tabs which could be used to change the local blade-section camber. For the tests described in this report, the trailing-edge tabs remained at 0° incidence.

The advanced set of model rotor blades was also 1/6-size and Mach scaled. The model-scale structural properties (table II) of the advanced blades, as

well as the distribution of these properties, were established as being representative of a full-scale design if such advanced blades were built. The advanced blades used RC(4)-10, RC(3)-10, and RC(3)-08 airfoils. The aerodynamic characteristics of the RC(3)-10 and RC(3)-08 airfoils are documented in reference 13. The aerodynamic characteristics of the RC(4)-10 airfoil have been obtained but have not yet been documented. The RC(4)-10 airfoil was used on the inboard portion of the blade to improve $C_{L,\max}$ characteristics on the retreating side of the rotor disk. The RC(3)-08 and RC(3)-10 airfoils were used on the outboard portion of the blade to increase the drag divergence Mach number in order to lessen compressibility effects on the advancing side of the rotor disk. The area, thrust-weighted, and torque-weighted solidities for the advanced rotor were 0.114, 0.101, and 0.0956, respectively. To evaluate blade modal shaping, each of the advanced blades was built with a magnesium block faired into the blade leading edge from $\frac{r}{R} = 0.566$ to $\frac{r}{R} = 0.637$. This block was hollow and allowed for the addition of nonstructural mass centered at $\frac{r}{R} = 0.600$. The nonstructural mass was added in the form of tungsten rods inserted chordwise into the magnesium block. Each tungsten rod had a nominal diameter of 0.25 in., a nominal length of 1.50 in., and a nominal mass of 0.00168 slug. A minimum of three and a maximum of seven tungsten rods could be added, with five tungsten rods being the "target" added mass. The five tungsten rods had a nominal mass of 0.00840 slug. During the modal shaping evaluation, nonstructural mass in the form of lead tape was added to the upper and lower surfaces of each blade at $\frac{r}{R} = 0.835$ to evaluate the addition of nonstructural mass at more than one blade radial station. The addition of the mass at each radial station was evaluated independently. The lead tape used at $\frac{r}{R} = 0.835$ was 2 in. in width and had a nominal mass of 0.00840 slug. The blade modal shaping evaluation was conducted independently of the rotor performance evaluation. Therefore, neither the tungsten weights nor the lead tape were added to the blades during the evaluation of rotor performance.

Each blade set was tested using the aeroelastic rotor experimental system (ARES) model shown in figures 5 and 6. The ARES model has a streamlined fuselage shape which encloses the rotor controls and drive system. The ARES model is powered by a variable-frequency synchronous motor rated at 47-hp output at 12 000 rpm. The motor is connected to the rotor shaft through a belt-driven two-stage speed reduction system. The ARES model rotor control system and rotor-shaft angle of attack are remotely controlled from the wind-tunnel control room. The model rotor-shaft angle of attack is varied by an electrically controlled hydraulic actuator. Blade collective pitch and lateral and longitudinal cyclic pitch are input to the rotor through the swash plate. The swash plate is moved by three hydraulic actuators.

Instrumentation mounted on the ARES model allows continuous displays of model control settings, rotor forces and moments, blade loads, and pitch-link loads. For these tests, one pitch link was instrumented with a strain gage to measure pitch-link tension and compression loads. Rotor-blade flap and lag motions are measured by rotary potentiometers mounted on the rotor hub and geared to the blade cuff. Rotor-shaft speed is determined by a magnetic sensor. The rotating-blade data are transferred through a 30-channel slip-ring assembly. Rotor forces and moments are measured by a six-component strain-gage balance mounted below the pylon and drive system. Rotor lift and drag are determined from the measured balance normal and axial forces (fig. 1). Rotor torque is measured by the balance yawing-moment channel. The balance is fixed with respect to the rotor shaft and pitches with the fuselage. Fuselage forces and moments are not sensed by the balance.

Test Procedure

The purpose of this test was to compare the performance and loads characteristics of the baseline and advanced-rotor systems. Therefore, both rotors were evaluated at the same nominal test conditions defined by μ, M_T, C_L, and C_D. The range of μ covered in these tests was from 0 to 0.40. In hover ($\mu = 0$), data were obtained at $z/d = 0.87$. To minimize rotor wake recirculation in hover, the tunnel floor and the model were lowered to provide a nominal 3-ft opening between the floor and tunnel walls. In forward flight, the values of M_T, C_L, and C_D were varied to represent simulated full-scale values of density altitude, vehicle gross weight, and rotor drag. The simulated rotor drag was determined at each velocity tested by using the vehicle equivalent parasite area as follows: $D = f_D(1/2\rho V^2)$. The simulated rotor drag coefficient was then determined from D. The values of density altitude, vehicle gross weight, and vehicle equivalent parasite area simulated with each rotor are presented in table III. At each test point, the rotor rotational speed and tunnel conditions were adjusted to give the desired values of M_T and μ. Model α_s and θ were then varied to obtain the desired values of C_L and C_D. To facilitate data acquisition and reduce blade loads, rotor cyclic pitch was used to remove rotor first-harmonic flapping with respect to the rotor shaft at each test point. The maximum obtainable values of μ, C_L, and C_D were constrained by either blade load limits or ARES model drive-system limits.

3

Model deadweight tares were determined throughout the range of shaft angle of attack with the blades installed and with them removed. Aerodynamic rotor-hub tares were determined with the blades removed throughout the ranges of shaft angle of attack and advance ratio investigated. Both deadweight and aerodynamic hub tares have been removed from the data presented herein. No corrections for tunnel wall effects have been applied to the data, but, as cited in reference 14, these effects are small for the flight conditions discussed herein.

Presentation of Results

The rotor performance data obtained during this investigation are presented as C_Q required to perform a given rotor task versus μ. The values of C_L and C_D used to define the rotor task, as well as C_Q, were obtained from the average of 2000 data samples taken over a nominal 20 rotor revolutions at each test condition. The C_Q data are presented for a series of full-scale values of vehicle gross weight, equivalent parasite area, and density altitude. Throughout the figures, the various density altitudes are denoted as a combination of geometric altitude and temperature, e.g., 4000 ft/95°F. The C_Q data as presented have not been divided by rotor solidity for two reasons. First, dividing by solidity does not account for all the effects due to differences in rotor solidity as discussed in reference 15. Second, the intent was to present gross differences in performance between two rotor designs, regardless of differences in solidity.

Loads data presented consist of pitch-link oscillatory load and fixed-system oscillatory load. The pitch-link and fixed-system oscillatory loads were obtained from a fast Fourier transform of the instrumented pitch-link and balance normal-force data for 12 rotor revolutions at each test condition. Pitch-link loads data are presented as normalized oscillatory (½ peak-to-peak) load versus μ. Fixed-system loads data are presented as normalized 4-per-rev vertical load versus μ. Just as for the performance data, the pitch-link and fixed-system loads data are presented for a series of full-scale vehicle gross weights, equivalent parasite areas, and density altitudes. All pitch-link oscillatory loads were normalized to the largest mean pitch-link oscillatory load measured on either rotor. All 4-per-rev fixed-system loads were normalized to the largest mean 4-per-rev fixed-system load generated by either rotor. This normalizing procedure was chosen because neither the fixed system nor the rotating system of the ARES model is a dynamically scaled representation of any existing helicopter. Therefore, scaling measured model data up to full-scale values would not be meaningful.

The quality of the performance data obtained during this investigation, with regard to repeatability, was addressed. During the test, 52 target data points were randomly selected to be repeated. The total number of actual repeat points was 102. The average deviation in C_L, C_D, and C_Q was determined from the differences between the target values and the repeated values. The average deviations for constant values of μ, α_s, θ, and rotor cyclic pitch were determined to be as follows:

$$C_L \pm 0.00004$$
$$C_D \pm 0.00001$$
$$C_Q \pm 0.00001$$

The data are presented in the following order:

	Figure
Rotor hover performance	7
Rotor forward-flight performance	8-11
Pitch-link oscillatory loads	12-16
Fixed-system oscillatory loads	17-22

Discussion of Results

The primary purpose of this investigation was to validate the advanced-blade aerodynamic design process by comparing the performance of the advanced rotor with that of the baseline rotor. The performance of each rotor was defined by the C_Q required at a given rotor task specified by the parameters C_L, C_D, μ, and M_T. The design philosophy used for the advanced blades was to produce a rotor that would be more efficient than the baseline rotor in both hover and forward flight, especially as the required rotor task became more demanding. Because of increased mission requirements for the UH-60A helicopter, rotor performance at a vehicle gross weight of 24 000 lb with a density altitude of 4000 ft/95°F was of particular interest. The baseline rotor was not originally designed to perform such a mission. The loads characteristics of each rotor, in terms of pitch-link loads and fixed-system oscillatory vertical loads, were also investigated. During the design process of the advanced rotor, the reduction of pitch-link loads and fixed-system loads was not directly addressed. However, it was hoped that a rotor could be produced with loads characteristics no worse than those of the baseline rotor.

Rotor Performance

Figure 7 is a comparison of the hover performance, in terms of C_L versus C_Q, of the baseline and advanced rotors at $M_T = 0.628$. This value of M_T is associated with density altitudes of SL/95°F and 4000 ft/95°F. The data were obtained at $z/d = 0.87$. The minimum C_L of interest in this figure is 0.00625, which is representative of the design gross weight

(16500 lb) of the UH-60A helicopter at SL/95°F. The data indicate that at $C_L = 0.00625$, there is no difference in performance between the baseline and advanced rotors. As C_L is increased above 0.00625, the performance of the advanced rotor improves relative to the baseline rotor. These higher values of rotor C_L are representative of higher vehicle gross weights and density-altitude conditions. Considering the higher solidity of the advanced rotor, it appears that the combination of airfoil section, twist, and taper have overcome the expected increases in rotor profile torque required in hover.

Figures 8 to 10 show the forward-flight performance of the baseline and advanced rotors, in terms of C_Q versus μ, for different gross weights and density altitudes at a constant value of f_D. The data show the improvement in performance provided by the advanced rotor at all test conditions. These performance improvements generally increase as the rotor task, defined by gross weight, density altitude, and μ, is increased. In some cases, the baseline rotor could not achieve the same rotor task as the advanced rotor because of increased rotor and fixed-system loads and because of excessive rotor power requirements. These baseline-rotor problems can most likely be attributed to retreating blade stall, which was alleviated on the advanced rotor by increased solidity and by the choice of airfoils used.

Figure 11 shows the effect of increasing f_D and density altitude on the performance of the advanced rotor. The increase in f_D and the high gross weight simulate the transportation of a large external load. The data show that this mission could be performed by the advanced rotor, with an increase in required C_Q, at least up to $\mu = 0.30$ and at a density altitude of 4000 ft/95°F.

Rotor and Fixed-System Loads

Figures 12 to 16 show the effects of gross weight, density altitude, and vehicle equivalent parasite area on pitch-link oscillatory loads for both the baseline and advanced rotors. The data indicate (figs. 12 to 14) that for constant f_D, the magnitude of the pitch-link oscillatory load produced by each rotor depends on the C_L (density altitude and gross weight) at which the rotor operates. Below a nominal $C_L = 0.00900$ (figs. 13(b) and 14(c)), the baseline rotor produces the lower pitch-link oscillatory load. Above the nominal $C_L = 0.00900$, the advanced rotor produces the lower pitch-link oscillatory load (figs. 14(d) to 14(f)). A closer examination of the data shows that the pitch-link oscillatory loads produced by the baseline rotor increase with C_L but those produced by the advanced rotor show no such large increase with C_L (fig. 15). This phenomenon indicates an

increasing level of torsional activity for the baseline blade as gross weight is increased. Reference 16 indicates that such torsional activity can contribute to reduced rotor performance. Figure 16 indicates that increasing f_D does not appreciably change the pitch-link oscillatory load for the advanced rotor. These results reinforce those of figures 12 to 14, which indicate that the advanced-rotor pitch-link oscillatory loads do not significantly increase when the rotor task is increased by increasing either gross weight or density altitude.

Figures 17 to 21 show the effects of gross weight, density altitude, and vehicle equivalent parasite area on the 4-per-rev fixed-system vertical loads produced by the baseline and advanced rotors. The data show that the 4-per-rev fixed-system loads produced by the advanced rotor are consistently higher than those produced by the baseline rotor for all test conditions. Figures 17 to 19 exhibit a trend in the 4-per-rev fixed-system loads data that is different from the trend with increasing C_L shown in figures 12 to 14 for the pitch-link oscillatory loads data. Pitch-link loads for the baseline rotor increased with C_L, while pitch-link loads for the advanced rotor remained relatively constant as C_L increased. However, with regard to 4-per-rev fixed-system loads, the loads produced by the baseline rotor tended to remain relatively constant, while the loads for the advanced rotor increased with C_L (fig. 20). These trends indicate different torsional loads characteristics and vertical hub shear characteristics for the baseline and advanced rotors. Figure 21 indicates that increasing f_D has no appreciable effect on the 4-per-rev fixed-system loads for the advanced rotor.

Figure 22 shows the results of an evaluation of blade modal shaping used to reduce fixed-system oscillatory loads. Modal shaping involves the addition of nonstructural mass to a blade to desensitize the response to selected harmonic aerodynamic loads generated by the blade. Pre-test analyses indicated that 4-per-rev fixed-system loads could be reduced by the addition of a nonstructural mass of 0.00839 slug to each of the advanced blades. During the tests, the addition of nonstructural mass at $\frac{r}{R} = 0.600$ and $\frac{r}{R} = 0.835$ was investigated. In figure 22, the measured 4-per-rev vertical fixed-system load is presented as a function of the amount of mass added to the advanced blades at both radial locations. The target mass of 0.00839 slug is represented in the figure by the addition of 5 masses to each blade. The data show that the addition of the 0.00839 slug at $\frac{r}{R} = 0.600$ had virtually no effect on the 4-per-rev vertical fixed-system loads for the advance ratios tested. The addition of more or less mass (7 or 3 masses, respectively) also had no effect on these

loads. Only one data point was obtained at $\mu = 0.15$ with the 0.00839-slug mass located at $\frac{r}{R} = 0.835$. This data point showed a reduction in the measured 4-per-rev vertical fixed-system loads compared with the case with the mass placed at $\frac{r}{R} = 0.600$. This evaluation of blade modal shaping is certainly not viewed as being conclusive, and further research in this area is planned for the future.

Conclusions

An investigation has been conducted in the Langley Transonic Dynamics Tunnel to evaluate differences between the performance and loads characteristics of a baseline rotor on the U.S. Army UH-60A helicopter and an advanced rotor for possible use on the same aircraft. The advanced rotor was designed to increase the mission capability of the UH-60A aircraft. Based on the data obtained for the test conditions and model configurations investigated, the following conclusions have been reached:

1. When compared with the baseline rotor, the advanced rotor provides performance improvements in hover above a rotor lift coefficient (C_L) of 0.00625 and at all forward-flight conditions, particularly at high gross weights and high density altitudes.

2. Oscillatory pitch-link loads produced by the baseline rotor increase with C_L, but those produced by the advanced rotor show no large variation with C_L.

3. The 4-per-rev vertical fixed-system loads produced by the advanced rotor are higher than those produced by the baseline rotor at all test conditions.

NASA Langley Research Center
Hampton, Virginia 23665-5225
June 17, 1987

References

1. Hammond, Charles Eugene; and Weller, William Henry: Wind-Tunnel Testing of Aeroelastically Scaled Helicopter Rotor Models. U.S. Army paper presented at the 1976 Army Science Conference (West Point, New York), June 22-25, 1976.

2. Popelka, David; Sheffler, Marc; and Bilger, Jim: Correlation of Stability Test Results and Analysis for the 1/5 Scale V-22 Aeroelastic Model. *41st Annual Forum Proceedings, American Helicopter Soc.*, c.1985, pp. 17–31.

3. Felker, Fort F.; and Light, Jeffrey S.: Rotor/Wing Aerodynamic Interactions in Hover. *42nd Annual Forum Proceedings, Volume I, American Helicopter Soc.,* c.1986, pp. 279–302.

4. Bingham, Gene J.: The Aerodynamic Influences of Rotor Blade Airfoils, Twist, Taper and Solidity on Hover and Forward Flight Performance. *Proceedings of the 37th Annual Forum, American Helicopter Soc.,* May 1981, pp. 37–50.

5. Gessow, Alfred; and Myers, Garry C., Jr.: *Aerodynamics of the Helicopter.* Macmillan Co., c.1952. (Republished 1967 by Frederick Ungar Publ. Co.)

6. Van Gaasbeek, J. R.: *Rotorcraft Flight Simulation, Computer Program C81—Volume II: User's Manual.* USARTL TR-77-54B, U.S. Army, Oct. 1979. (Available from DTIC as AD A079 632.)

7. Taylor, Robert B.: Helicopter Vibration Reduction by Rotor Blade Modal Shaping. *38th Annual Forum Proceedings, American Helicopter Soc.,* 1982, pp. 90–101.

8. Lee, Charles: *Weight Considerations in Dynamically Similar Model Rotor Design.* SAWE Paper No. 659, May 1968.

9. Johnson, Wayne: *A Comprehensive Analytical Model of Rotorcraft Aerodynamics and Dynamics. Part I: Analysis Development.* NASA TM-81182, AVRADCOM TR-80-A-5, 1980.

10. Johnson, Wayne: *A Comprehensive Analytical Model of Rotorcraft Aerodynamics and Dynamics. Part II: User's Manual.* NASA TM-81183, AVRADCOM TR-80-A-6, 1980.

11. Blackwell, R. H.; Murrill, R. J.; Yeager, W. T., Jr.; and Mirick, P. H.: Wind Tunnel Evaluation of Aeroelastically Conformable Rotors. Preprint No. 80-23, American Helicopter Soc., May 1980.

12. Noonan, Kevin W.; and Bingham, Gene J.: *Aerodynamic Characteristics of Three Helicopter Rotor Airfoil Sections at Reynolds Numbers From Model Scale to Full Scale at Mach Numbers From 0.35 to 0.90.* NASA TP-1701, AVRADCOM TR-80-B-5, 1980.

13. Bingham, Gene J.; and Noonan, Kevin W.: *Two-Dimensional Aerodynamic Characteristics of Three Rotorcraft Airfoils at Mach Numbers From 0.35 to 0.90.* NASA TP-2000, AVRADCOM TR-82-B-2, 1982.

14. Mantay, Wayne R.; Yeager, William T., Jr.; Hamouda, M-Nabil; Cramer, Robert G., Jr.; and Langston, Chester W.: *Aeroelastic Model Helicopter Rotor Testing in the Langley TDT.* NASA TM-86440, USAAVSCOM TM-85-B-5, 1985.

15. Yeager, William T., Jr.; and Mantay, Wayne R.: *Correlation of Full-Scale Helicopter Rotor Performance in Air With Model-Scale Freon Data.* NASA TN D-8323, 1976.

16. Mantay, Wayne R.; and Yeager, William T., Jr.: *Parametric Tip Effects for Conformable Rotor Applications.* NASA TM-85682, AVRADCOM TR-83-B-4, 1983.

Table I. Baseline-Rotor-Blade Properties

(a) Structural properties

Inboard section, r/R	Section length, ft	Section mass, slugs	Stiffness, lb-ft^2			I_θ, lb-sec^2
			Flap	Chord	Torsion	
0.0534	0.322	0.0510	101 944.0	104 166.7	6 763.9	0.570×10^{-3}
.1222	.166	.0110	9 326.4	69 444.4	1 269.6	.143
.1577	.333	.0062	9 326.4	2 777.8	432.1	.050
.2288	.333	.0062	74.3	2 777.8	236.1	.050
.2999	.333	.0062	74.3	2 777.8	88.9	.050
.3710	.333	.0062	74.3	2 777.8	88.9	.080
.4421	.333	.0062	81.3	2 777.8	91.6	.080
.5132	.333	.0062	75.7	2 777.8	93.1	.080
.5843	.333	.0062	81.3	2 777.8	94.4	.080
.6554	.333	.0062	81.3	2 777.8	94.4	.080
.7265	.333	.0062	81.3	2 777.8	94.4	.080
.7976	.333	.0062	86.8	2 777.8	92.4	.080
.8687	.207	.0054	33.3	694.4	95.4	.117
.9128	.073	.0024	33.3	694.4	27.1	.117
.9283	.336	.0045	21.5	347.2	22.0	.117

(b) Model rotor-blade rotating natural frequencies

Modal identity	ω/Ω^1
Flap	2.69
Flap	4.76
Chord	5.12
Torsion	7.21
Flap	8.16

[1]$\Omega = 69.32$ rad/sec.

Table II. Advanced-Rotor-Blade Properties

(a) Structural properties

Inboard section. r/R	Section length, ft	Section mass, slugs	Stiffness, lb-ft^2			I_θ, lb-sec^2
			Flap	Chord	Torsion	
0.0534	0.1070	0.02460	101 944.0	104 166.7	6 763.9	0.570×10^{-3}
.0763	.2150	.03400	101 944.0	104 166.7	6 763.9	.190
.1221	.0005	.00004	101 944.0	104 166.7	6 763.9	.190
.1222	.1770	.00410	2 500.0	10 277.8	12 625.0	.242
.1600	.2480	.00430	354.1	10 277.8	261.1	.242
.2130	.1690	.00260	302.1	10 277.8	261.1	.226
.2490	.5200	.01220	270.1	10 277.8	261.1	.359
.3600	.9650	.02260	225.7	10 277.8	261.1	.359
.5659	.3330	.00790	225.7	10 277.8	261.1	.359
.6370	.0420	.00100	295.1	10 277.8	428.8	.228
.6460	.2670	.00670	258.3	10 277.8	288.2	.359
.7030	.4120	.01030	251.7	10 277.8	270.8	.373
.7910	.3370	.00780	236.1	10 277.8	256.9	.359
.8630	.3320	.00670	138.9	10 277.8	217.7	.305
.9340	.2060	.00270	79.9	10 277.8	163.2	.140
.9780	.1030	.00076	62.5	10 277.8	86.8	.074

(b) Model rotor-blade rotating natural frequencies

Modal identity	ω/Ω[1]
Flap	2.86
Flap	5.71
Chord	8.46
Flap	9.90

[1] $\Omega = 69.32$ rad/sec.

Table III. Forward-Flight Test Matrix for Baseline and Advanced Rotors

Rotor task			Figure			M_T	μ
Gross weight, lb	Density altitude	f_D, ft^2	C_Q vs μ	PL vs μ	FSO_{4p} vs μ		
18500	SLS	29.94	8	12	17	0.65	0.15–.40
18500	SL/95°F		9(a)	13(a)	18(a)	.628	.15 .40
24000	SL/95°F		9(b)	13(b)	18(b)		.15–.35
16500	4000 ft/95°F		10(a)	14(a)	19(a)		.15–.40
18500			10(b)	14(b)	19(b)		.15 .40
20500			10(c)	14(c)	19(c)		.15–.37
22500			10(d)	14(d)	19(d)		.15–.37
24500			10(e)	14(e)	19(e)		.15–.37
26500			10(f)	14(f)	19(f)		.15–.30
^{a}24000	SL/95°F	89.94	11(a)	16(a)	21(a)		.15–.35
^{a}24000	4000 ft/95°F	89.94	11(b)	16(b)	21(b)		.15–.35

^{a}Indicates test condition for advanced rotor only.
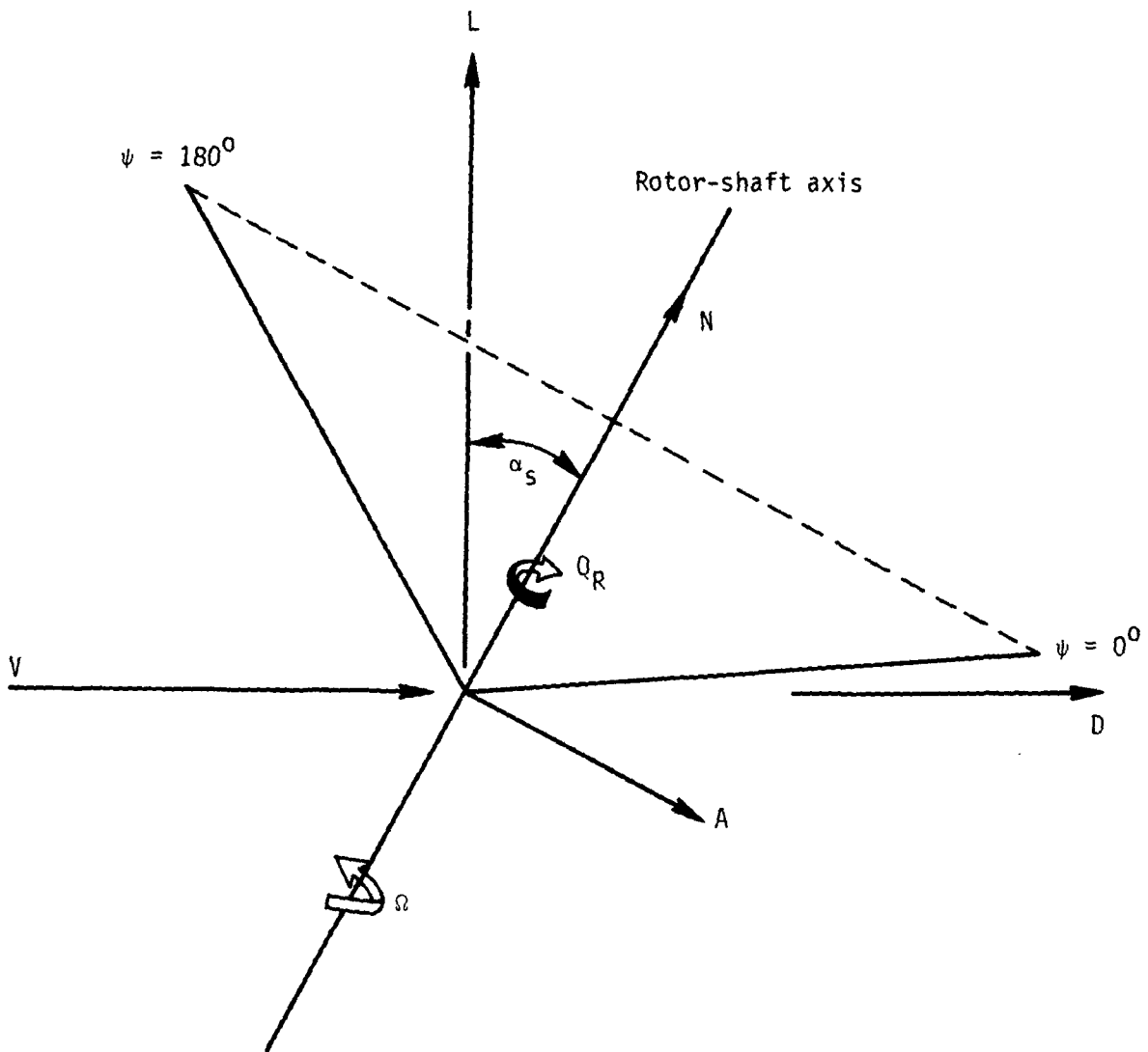
Figure 1. Notation showing positive directions of forces, angles, and velocities.
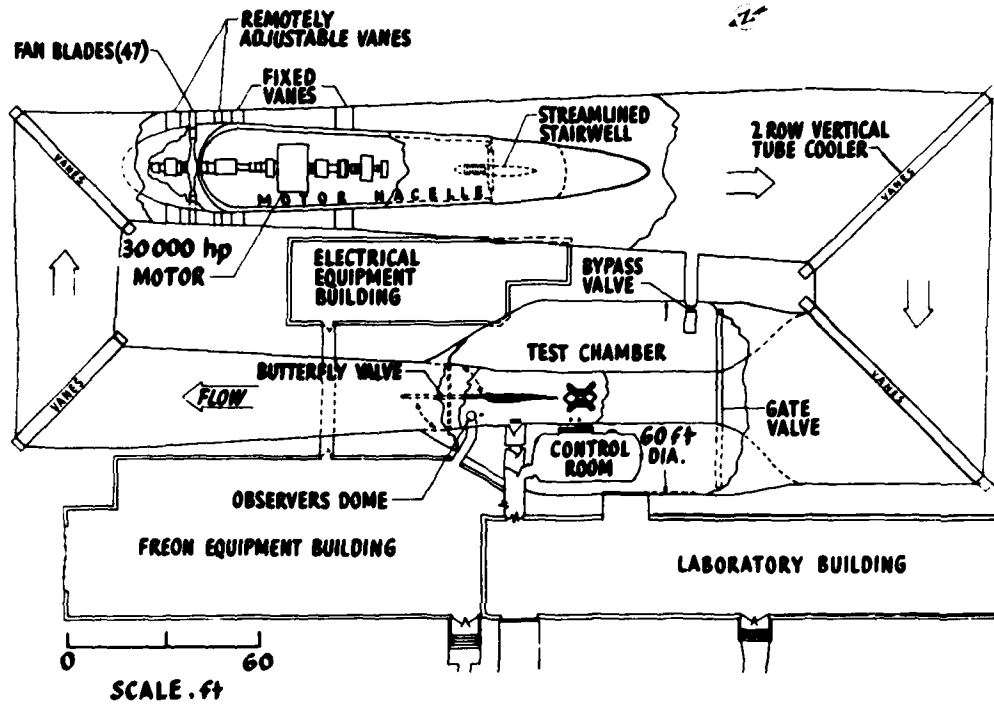
(a) Tunnel planform.
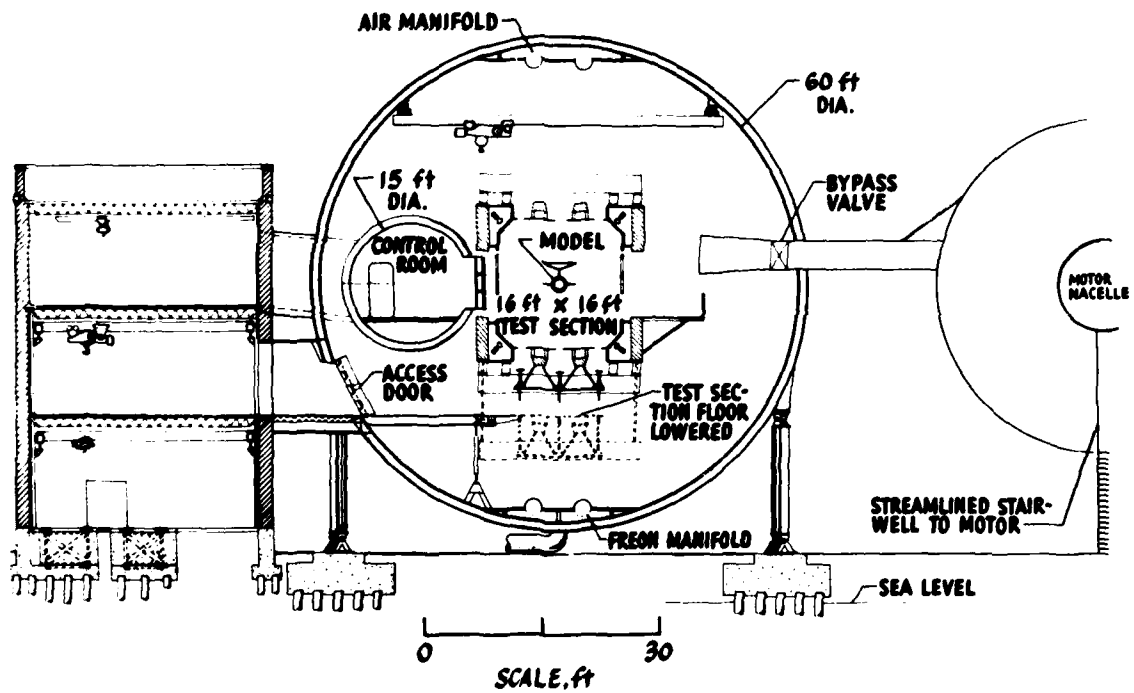
(b) Tunnel cross section.

Figure 2. Langley Transonic Dynamics Tunnel.
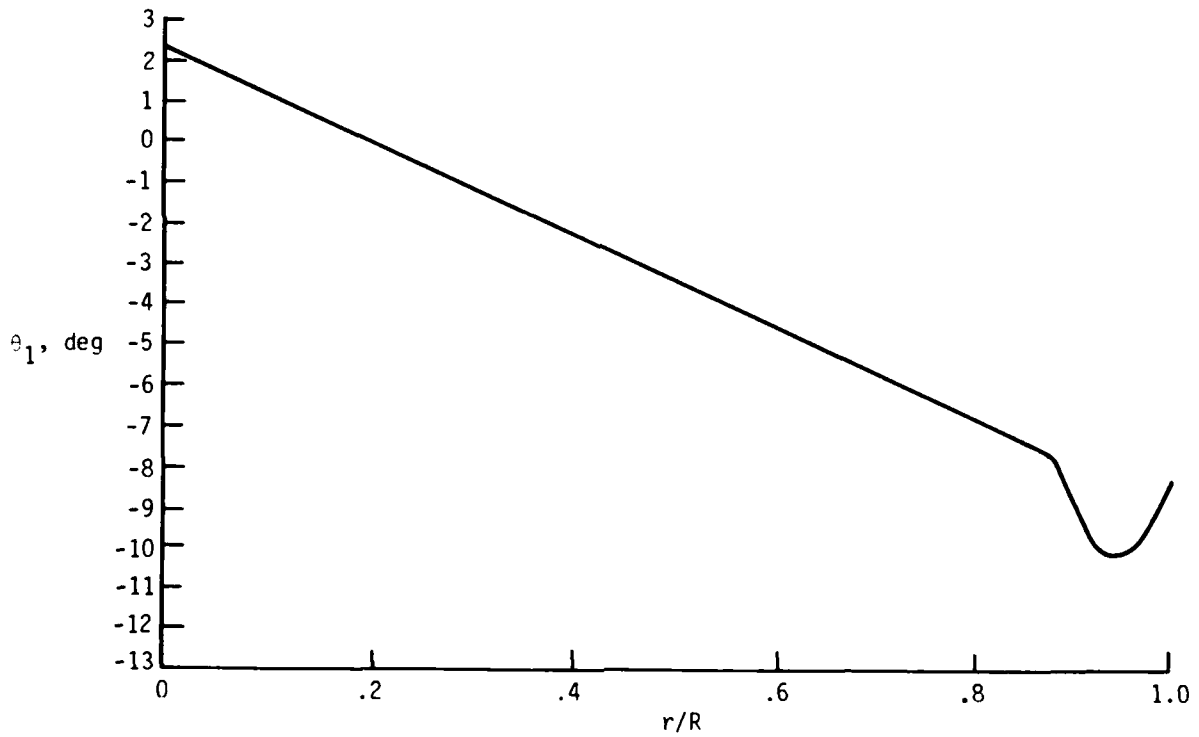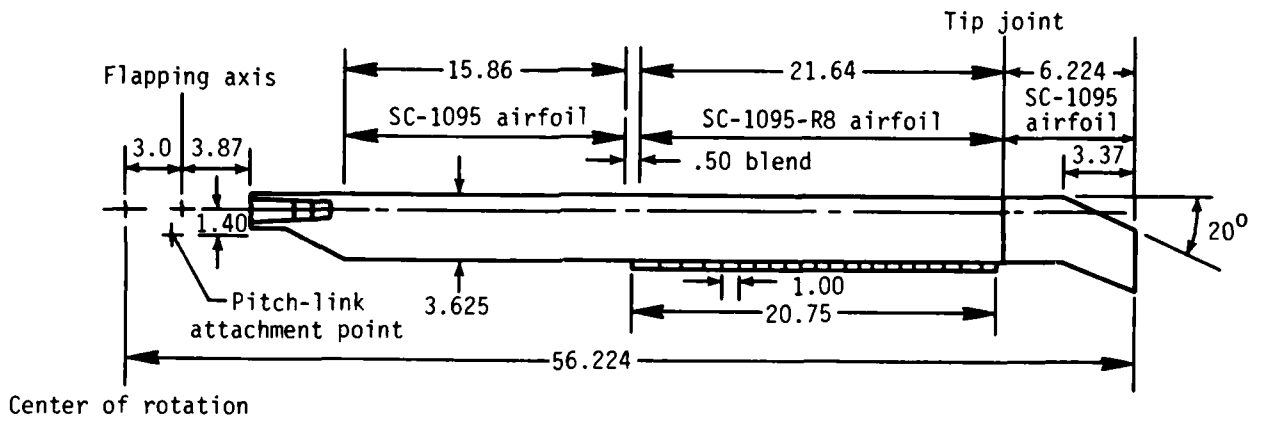
Figure 3. Baseline-rotor-blade geometry and built-in twist distribution. Linear dimensions are in inches.
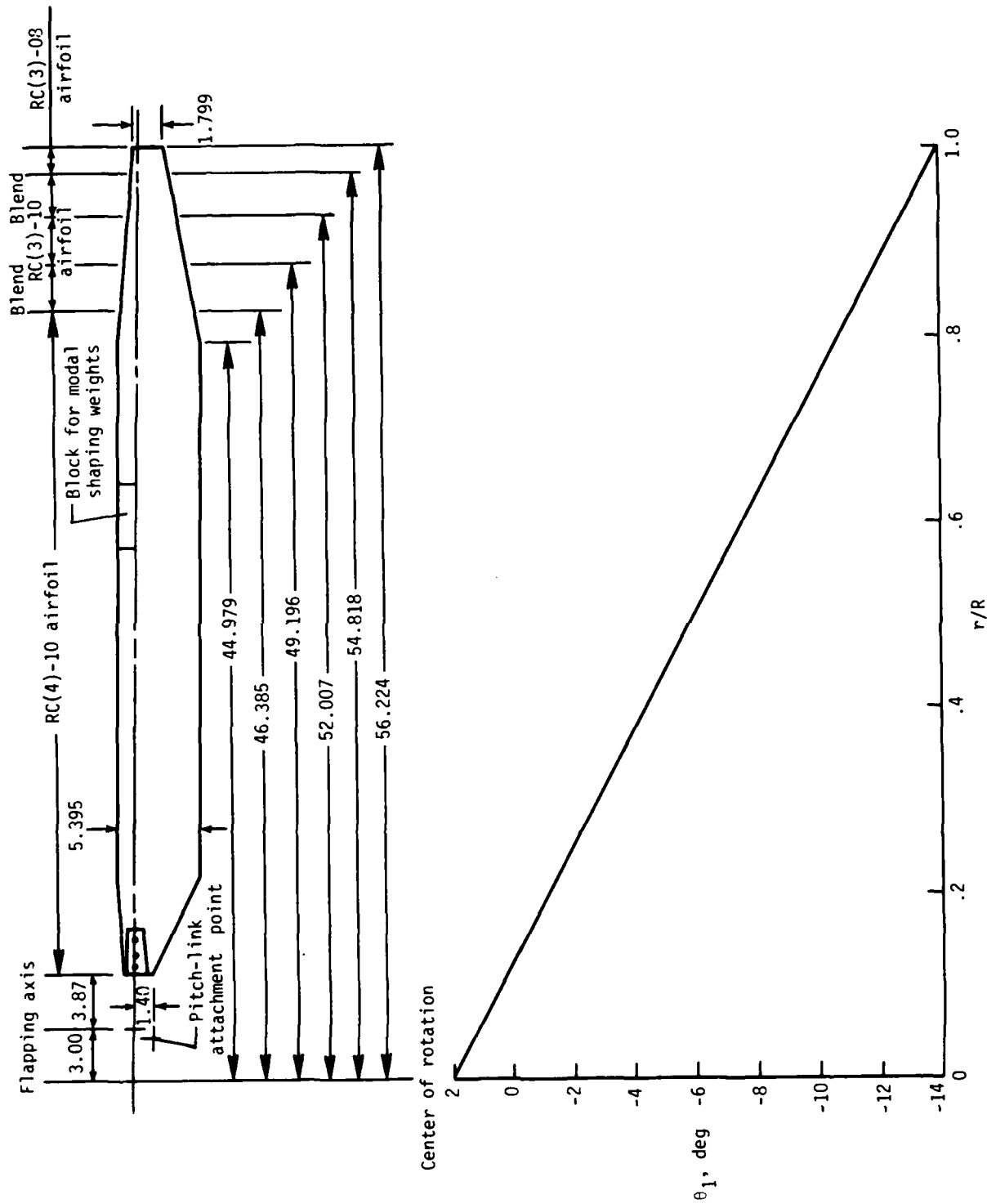
Figure 4. Advanced-rotor-blade geometry and built-in twist distribution. Linear dimensions are in inches.
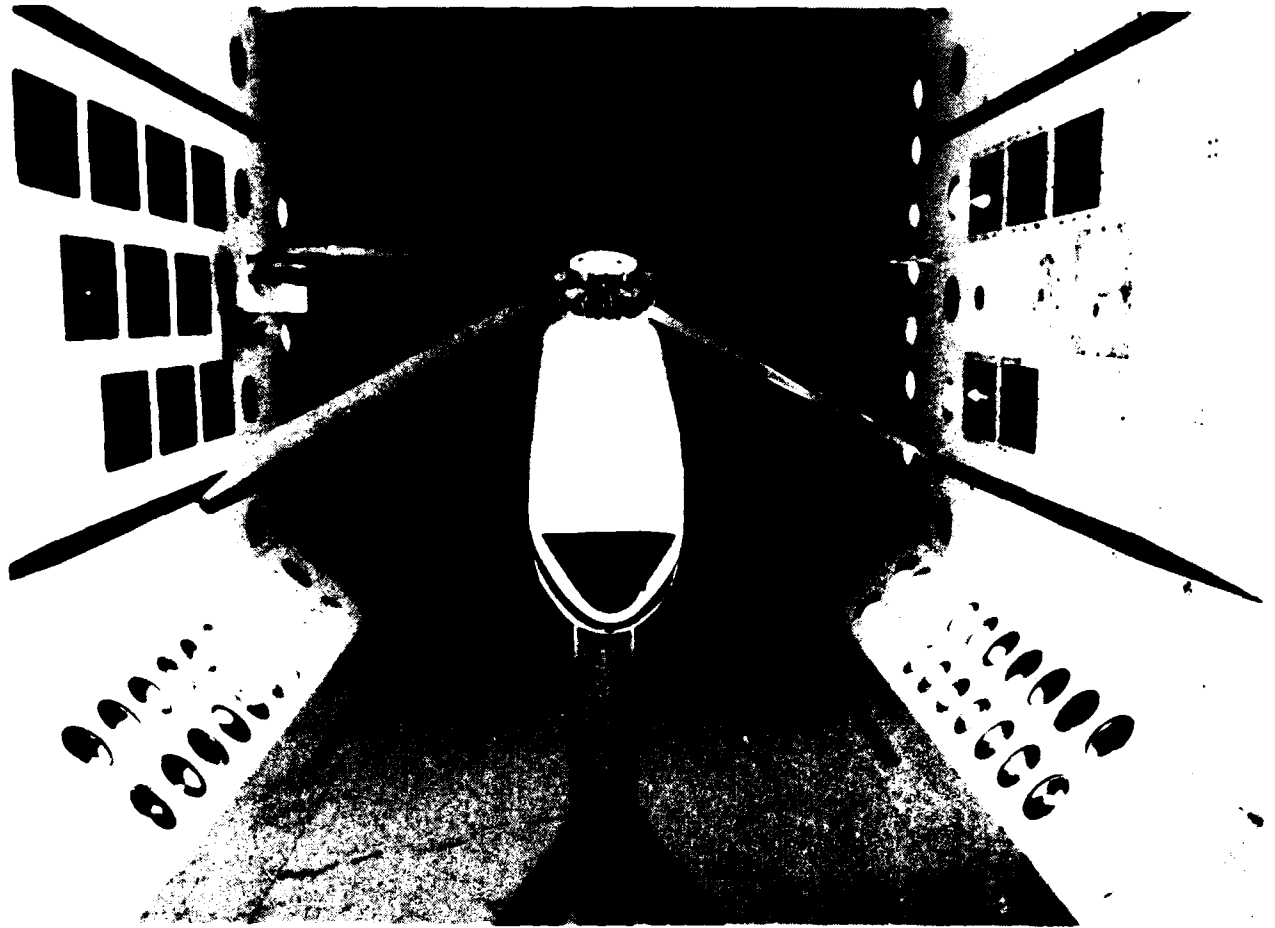
L-85-12.990

Figure 5. Aeroelastic rotor experimental system model in Langley Transonic Dynamics Tunnel.
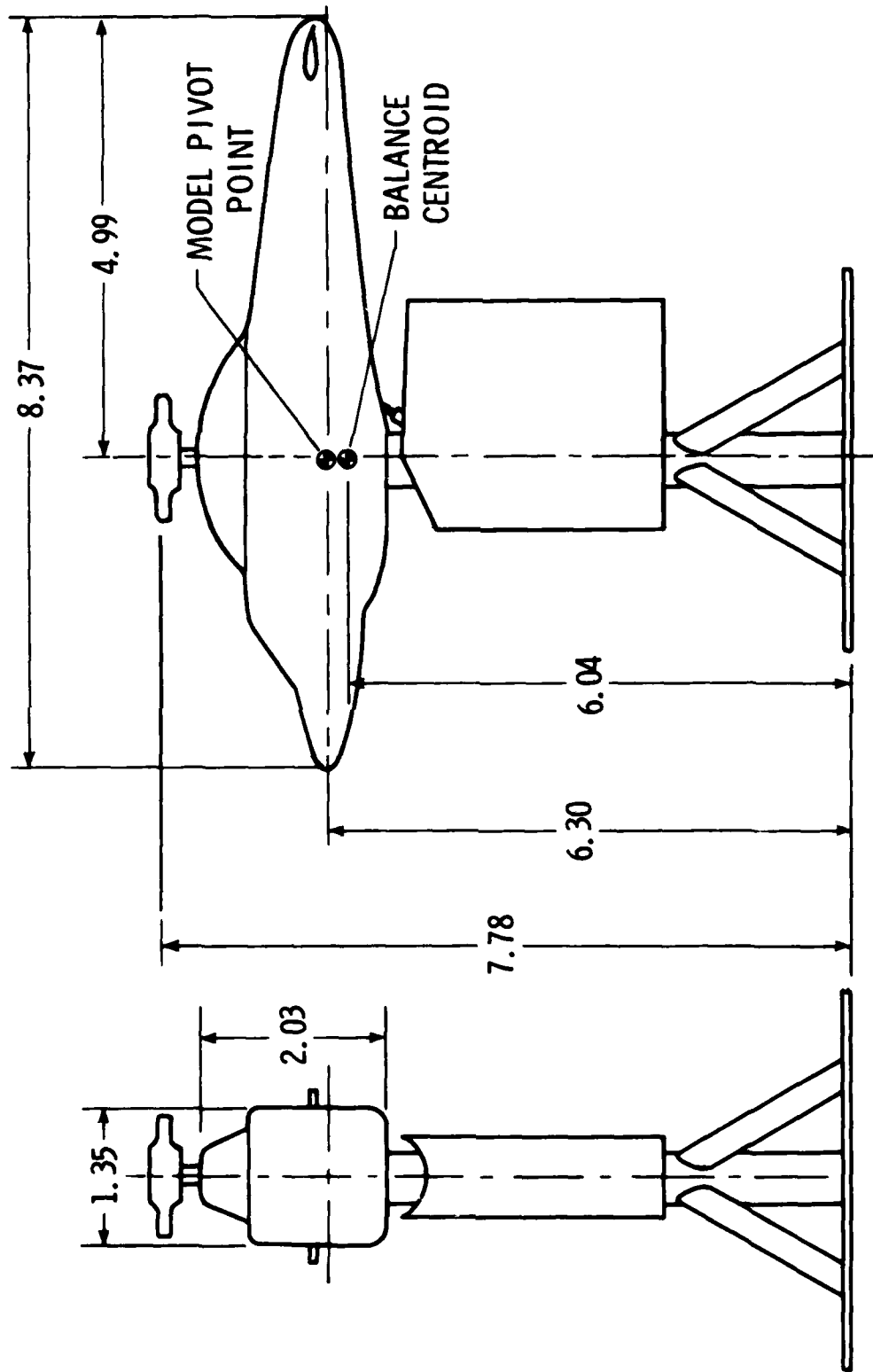
Figure 6. Schematic of aeroelastic rotor experimental system model. All dimensions are in feet.
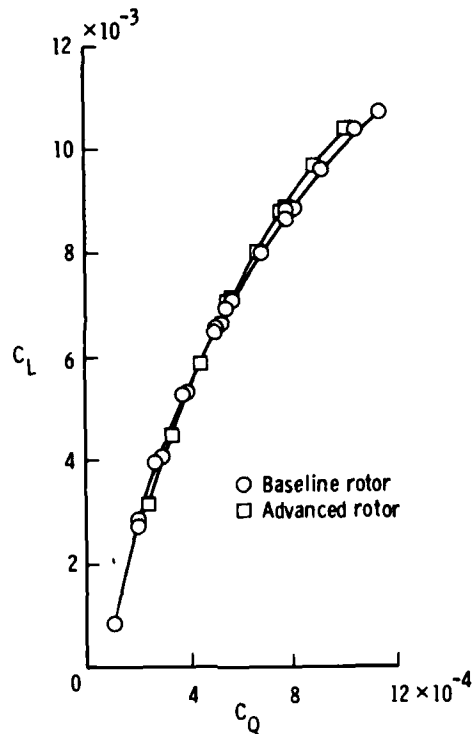
Figure 7. Comparison of hover performance of baseline and advanced rotors at $M_T = 0.628$ and $z/d = 0.87$.
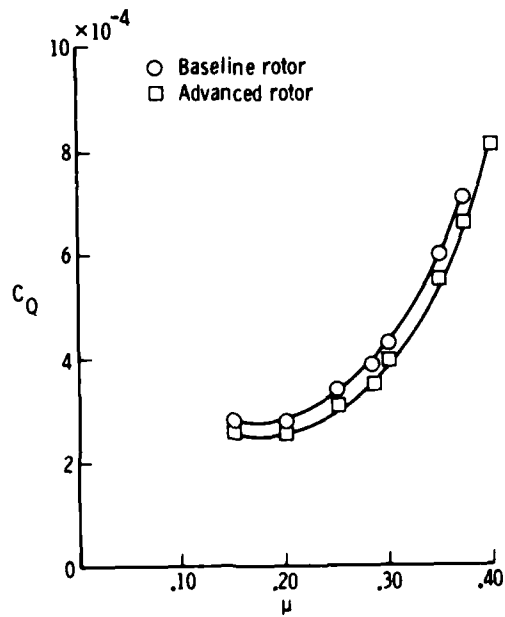
Figure 8. Comparison of baseline- and advanced-rotor C_Q at a gross weight of 18 500 lb ($C_L = 0.00654$), SLS, and $f_D = 29.94$ ft^2.
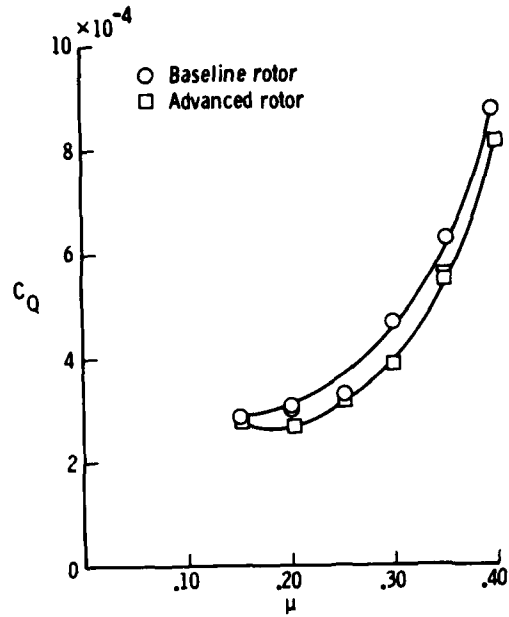
(a) Gross weight = 18 500 lb; C_L = 0.00701.
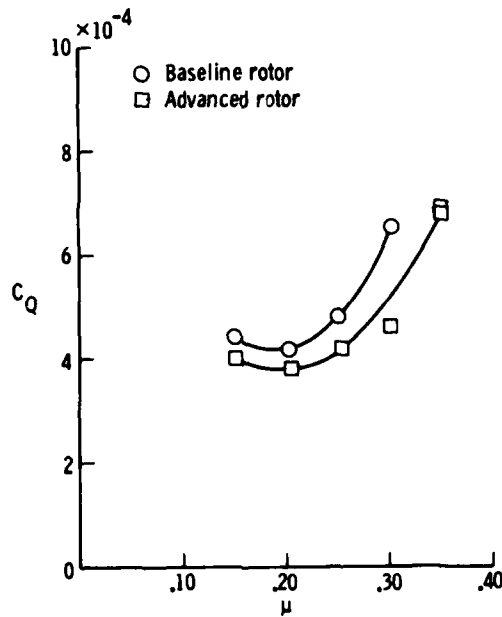
(b) Gross weight = 24 000 lb; C_L = 0.00909.

Figure 9. Comparison of baseline- and advanced-rotor C_Q at SL/95°F and f_D = 29.94 ft^2.
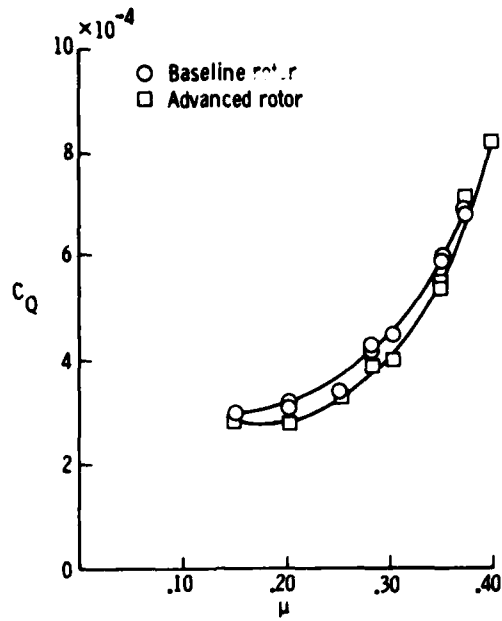
(a) Gross weight = 16 500 lb; $C_L = 0.00723$.
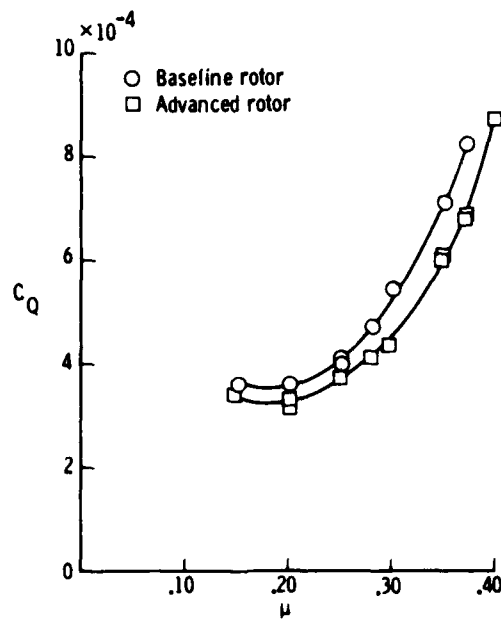
(b) Gross weight = 18 500 lb; $C_L = 0.00810$.

Figure 10. Comparison of baseline- and advanced-rotor C_Q for a density altitude of 4000 ft/95°F and $f_D = 29.94$ ft^2.
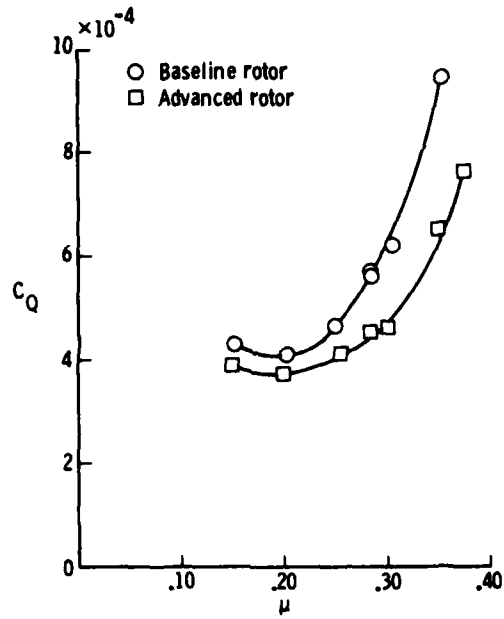
(c) Gross weight = 20 500 lb; $C_L = 0.00898$.
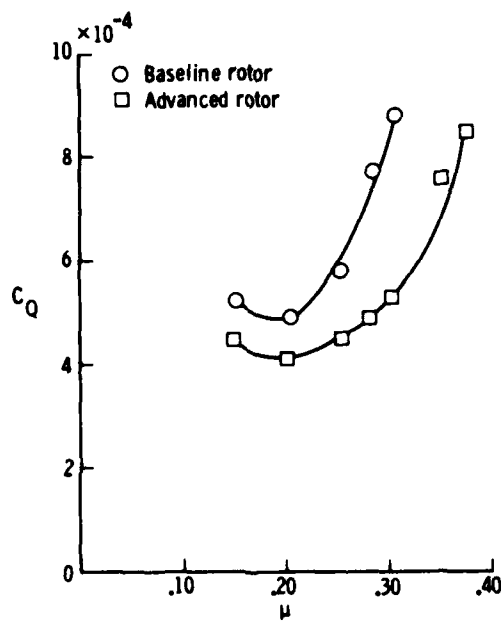
(d) Gross weight = 22 500 lb; $C_L = 0.00985$.

Figure 10. Continued.
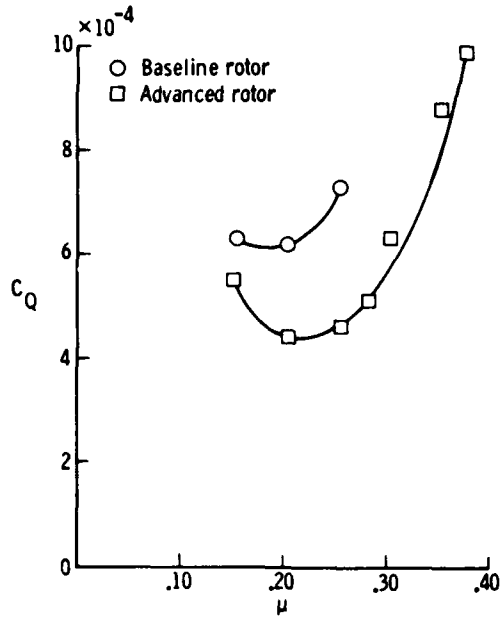
(e) Gross weight = 24 500 lb; $C_L = 0.0107$.
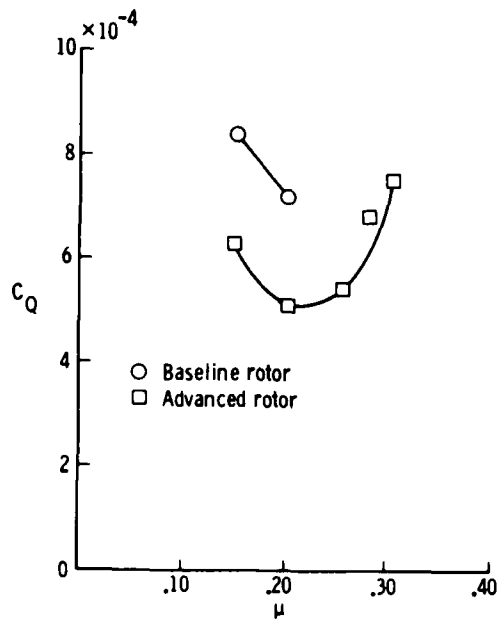
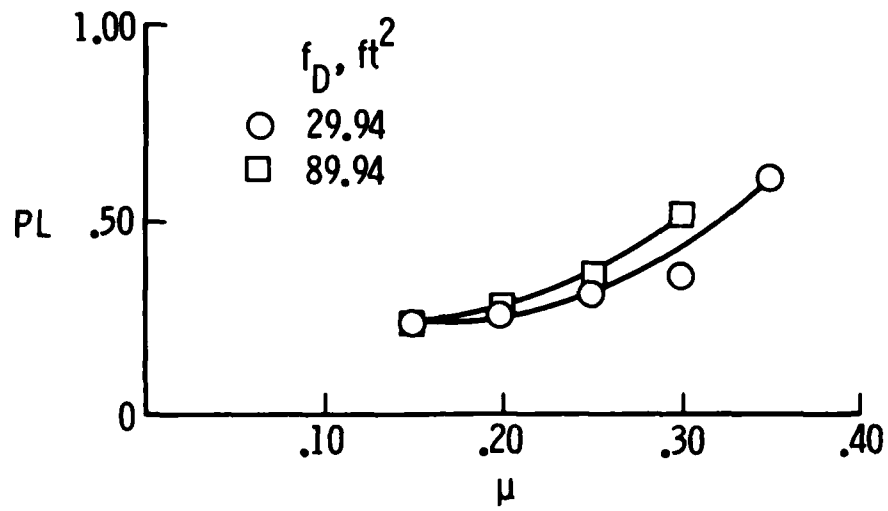(f) Gross weight = 26 500 lb; $C_L = 0.0116$.

Figure 10. Concluded.
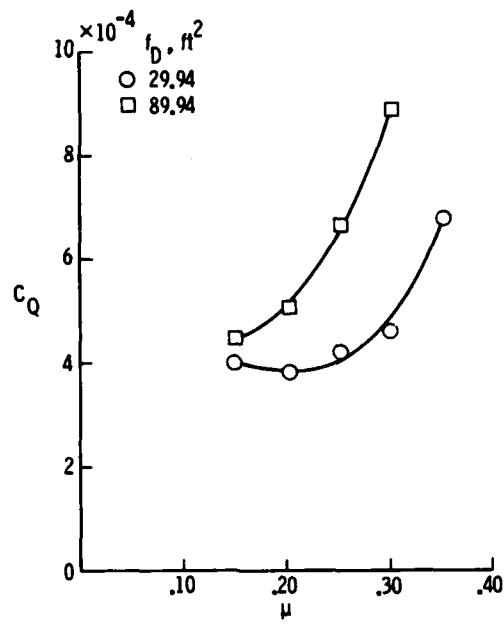
(a) SL/95°F; $C_L = 0.00909$.
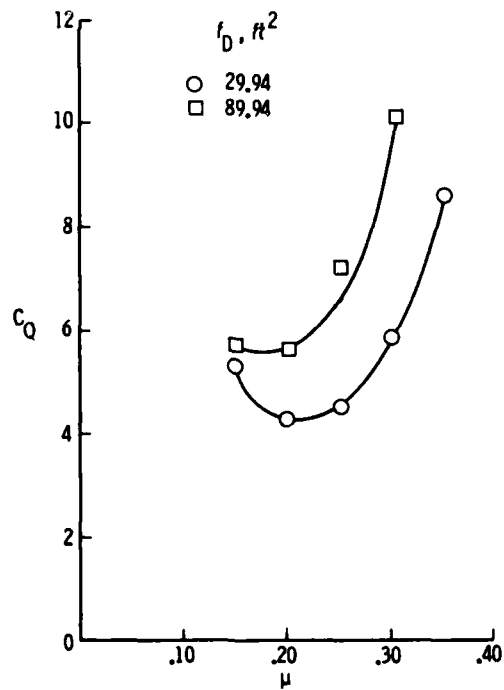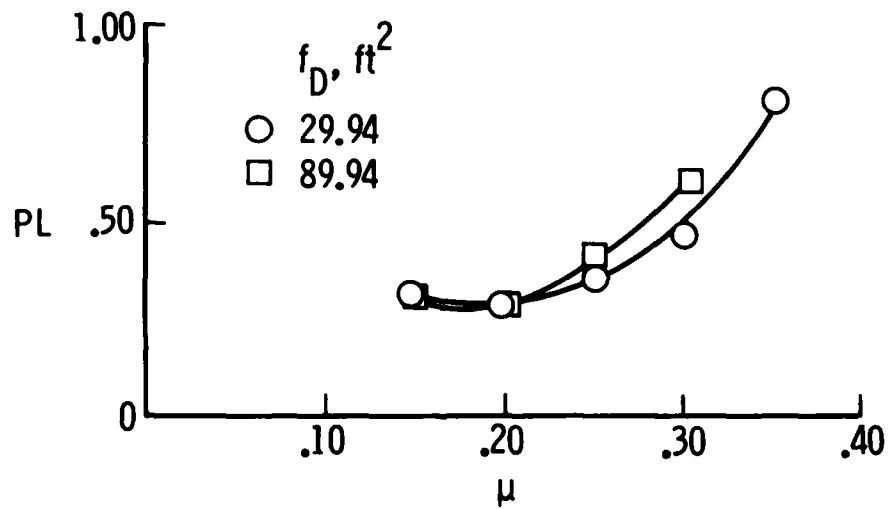

(b) 4000 ft/95°F; $C_L = 0.0105$.

Figure 11. Effect of vehicle flat-plate drag on advanced-rotor performance at a gross weight of 24 000 lb.
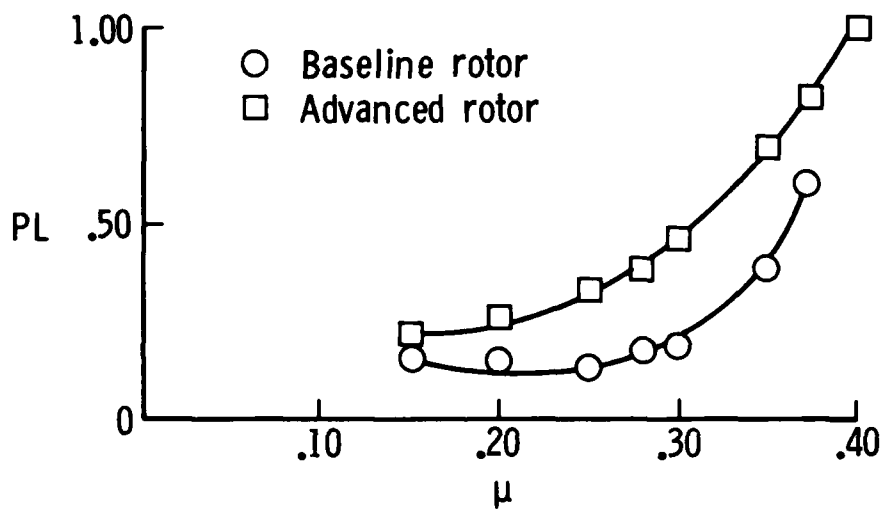
Figure 12. Comparison of baseline- and advanced-rotor normalized pitch-link oscillatory load (½ peak-to-peak) at a gross weight of 18 500 lb ($C_L = 0.00654$), SLS, and $f_D = 29.94$ ft^2.
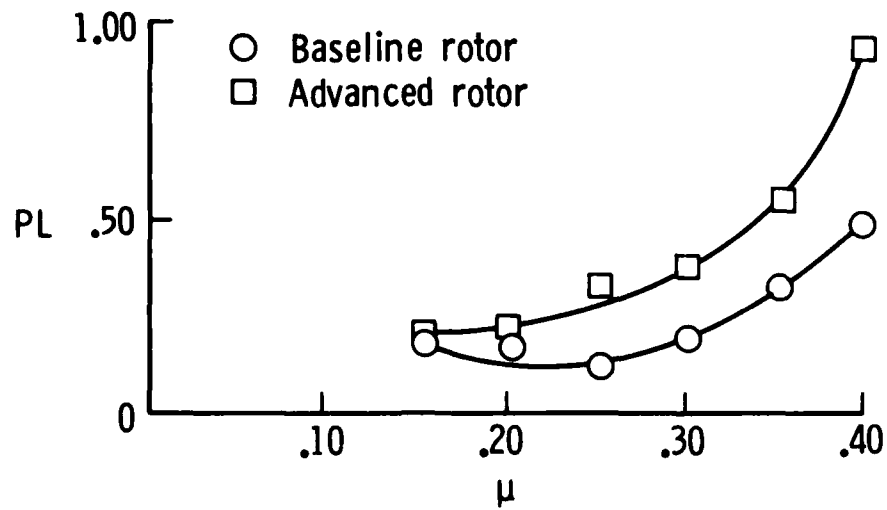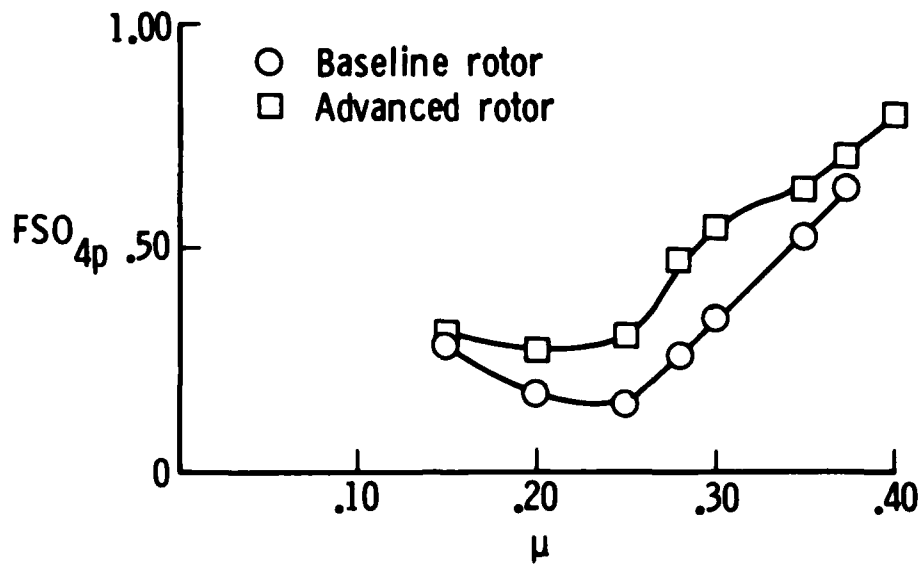
(a) Gross weight = 18 500 lb; C_L = 0.00701.
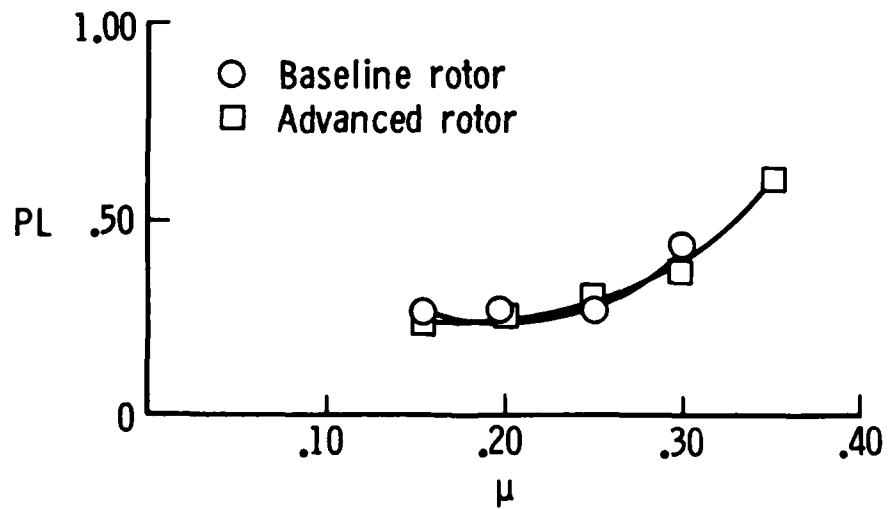
(b) Gross weight = 24 000 lb; C_L = 0.00909.

Figure 13. Comparison of baseline- and advanced-rotor normalized pitch-link oscillatory load ($\frac{1}{2}$ peak-to-peak) at SL/95°F and f_D = 29.94 ft^2.
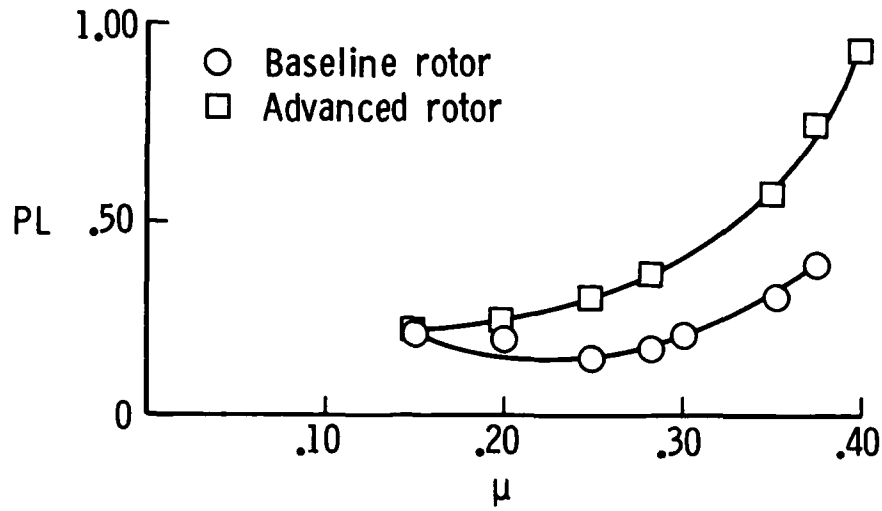
(a) Gross weight = 16 500 lb; $C_L = 0.00723$.
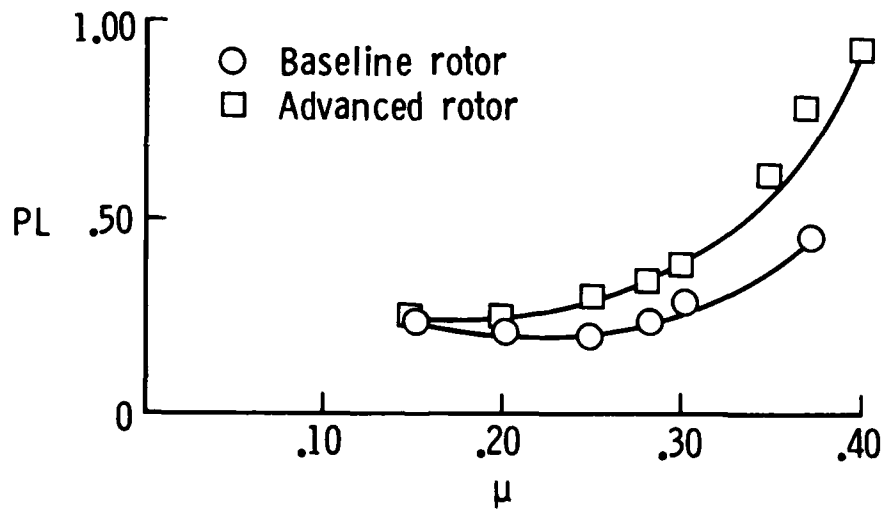
(b) Gross weight = 18 500 lb; $C_L = 0.00810$.

Figure 14. Comparison of baseline- and advanced-rotor normalized pitch-link oscillatory load (½ peak-to-peak) at 4000 ft/95°F and $f_D = 29.94$ ft^2.
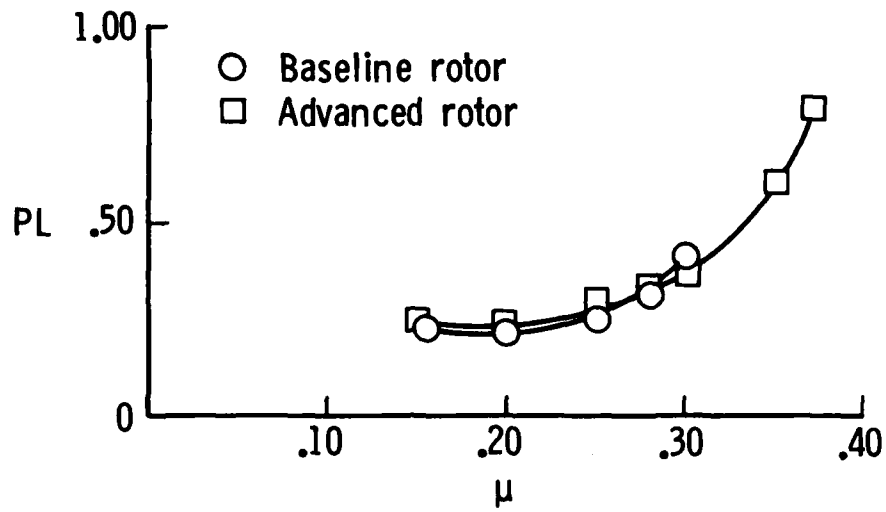
(c) Gross weight = 20 500 lb; $C_L = 0.00898$.
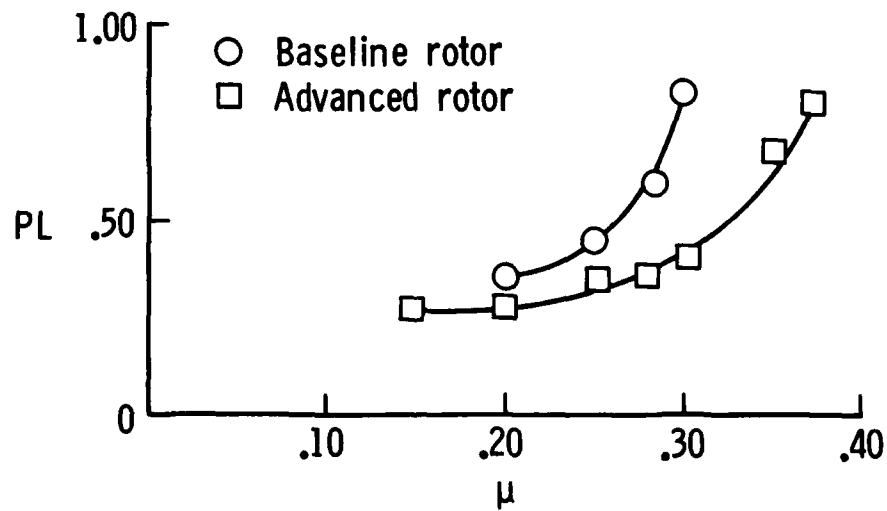
(d) Gross weight = 22 500 lb; $C_L = 0.00985$.

Figure 14. Continued.
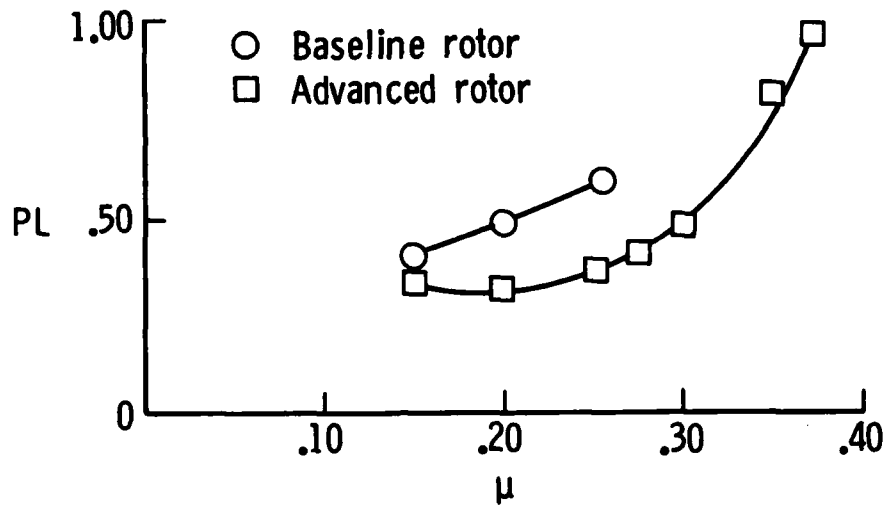
(e) Gross weight = 24 500 lb; $C_L = 0.0107$.
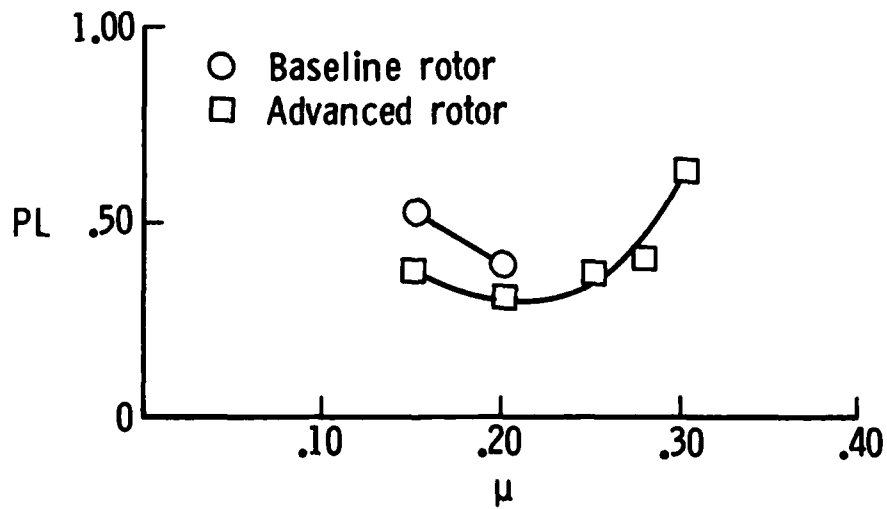
(f) Gross weight = 26 500 lb; $C_L = 0.0116$.

Figure 14. Concluded.
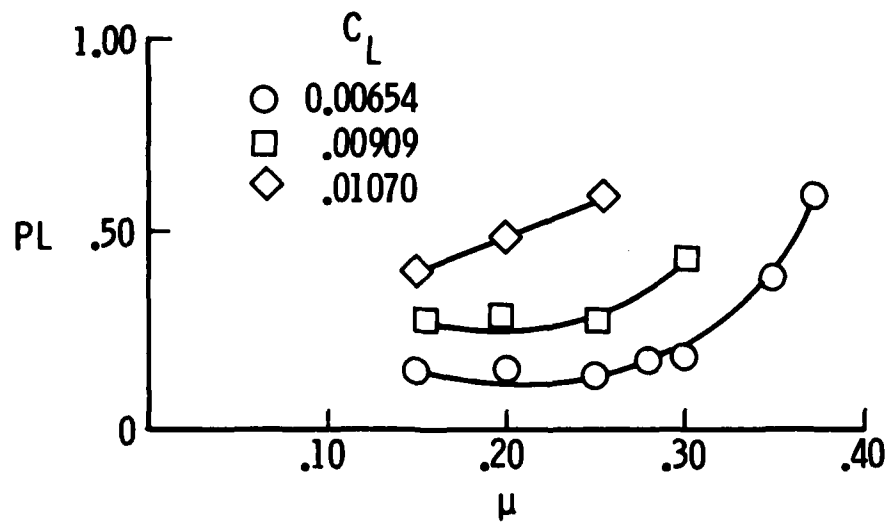
(a) Baseline rotor.
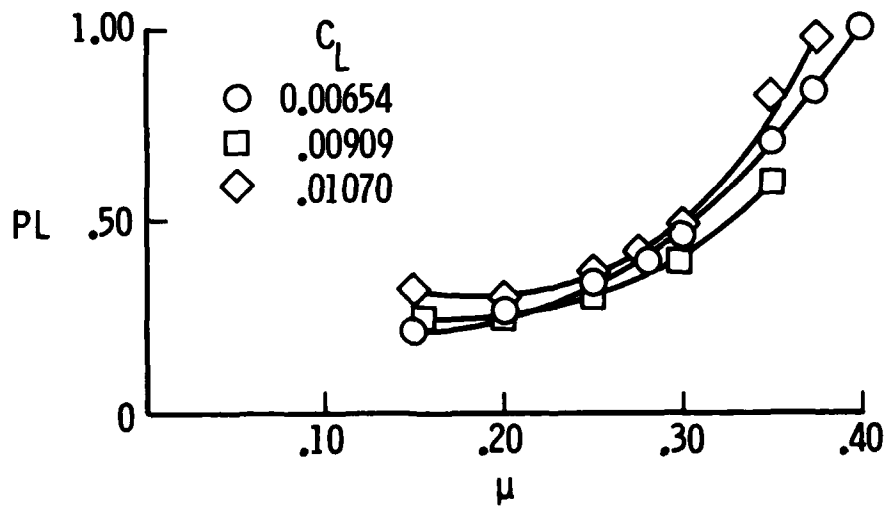
(b) Advanced rotor.

Figure 15. Effect of C_L on rotor normalized pitch-link oscillatory load ($\frac{1}{2}$ peak-to-peak) for $f_D = 29.94$ ft^2.

(a) SL/95°F: $C_L = 0.00909$.

(b) 4000 ft/95°F: $C_L = 0.0105$.

Figure 16. Effect of vehicle flat-plate drag on advanced-rotor pitch-link oscillatory load ($\frac{1}{2}$ peak-to-peak) at a gross weight of 24 000 lb.
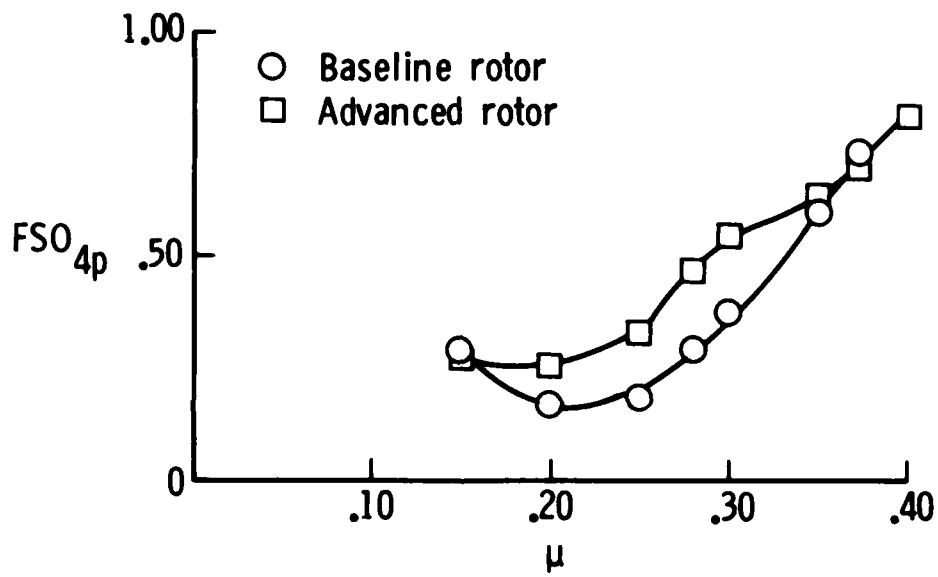
Figure 17. Comparison of 4-per-rev fixed-system loads for baseline- and advanced-rotor configurations at a gross weight of 18500 lb ($C_L = 0.000654$), SLS, and $f_D = 29.94$ ft^2.
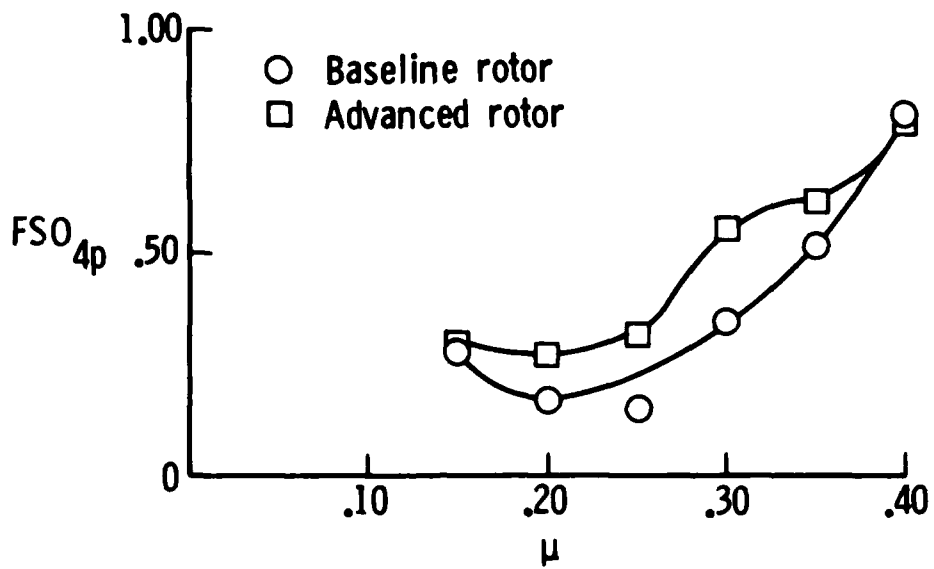
(a) Gross weight = 18 500 lb; C_L = 0.00701.
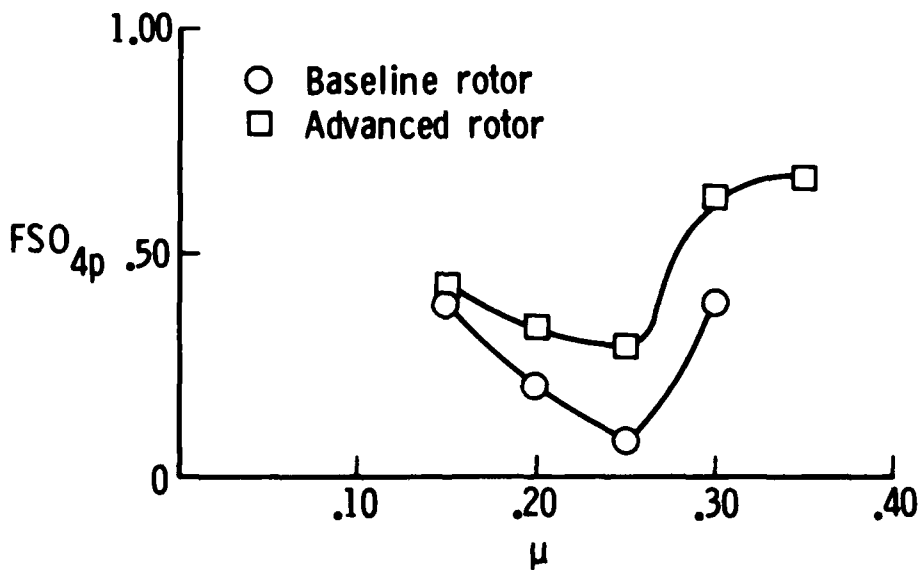
(b) Gross weight = 24 000 lb; C_L = 0.00909.

Figure 18. Comparison of 4-per-rev fixed-system loads for baseline- and advanced-rotor configurations at SL/95°F and f_D = 29.94 ft^2.
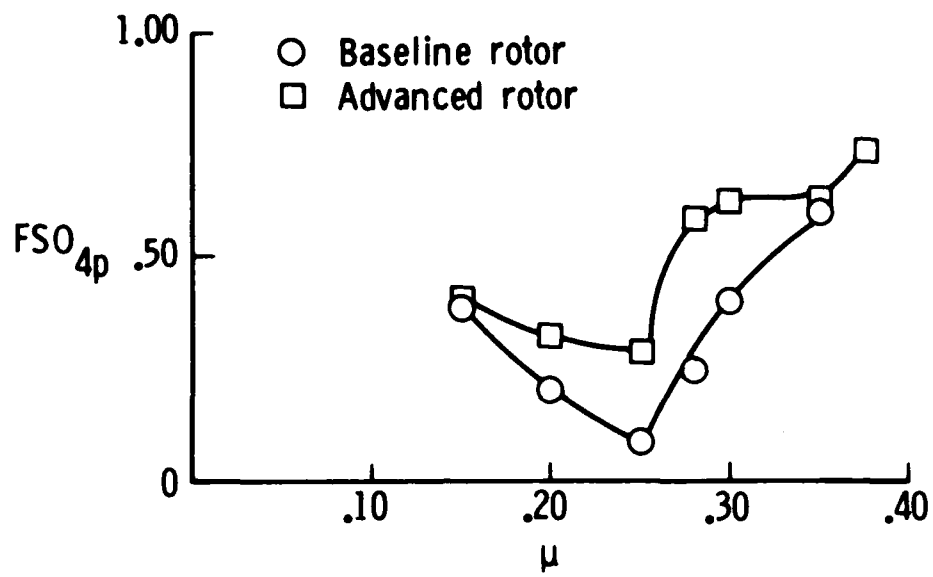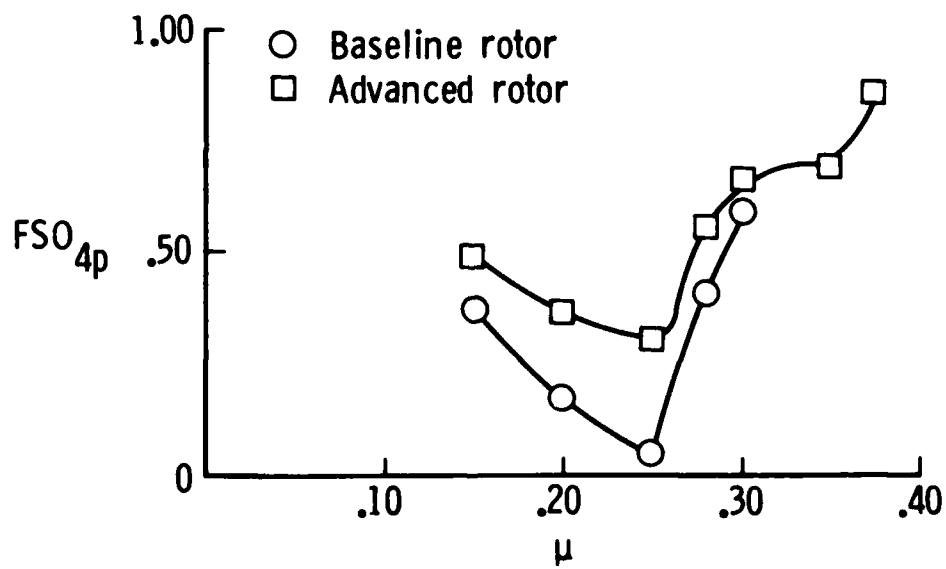
(a) Gross weight = 16 500 lb; C_L = 0.00723.
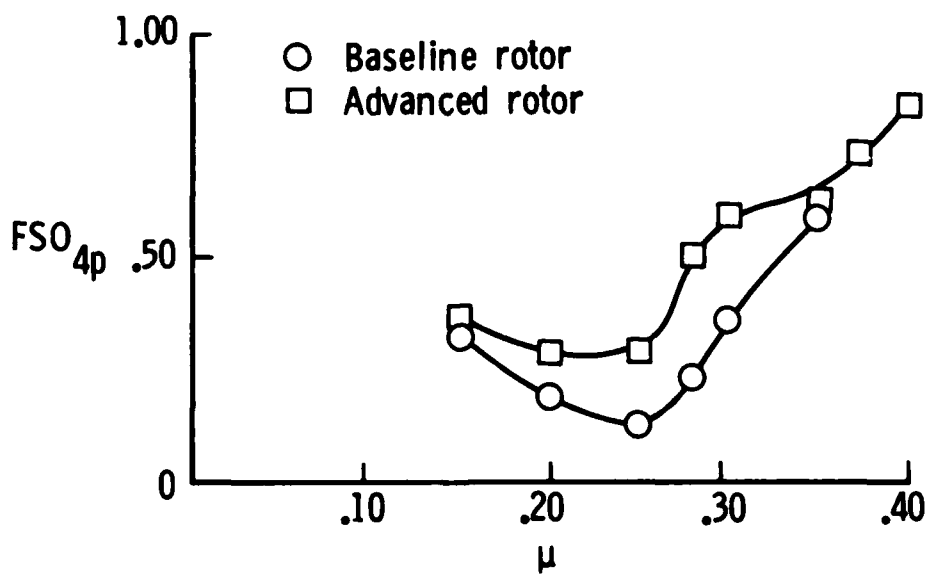
(b) Gross weight = 18 500 lb; C_L = 0.00810.

Figure 19. Comparison of 4-per-rev fixed-system loads for baseline- and advanced-rotor configurations at 4000 ft/95°F and f_D = 29.94 ft^2.
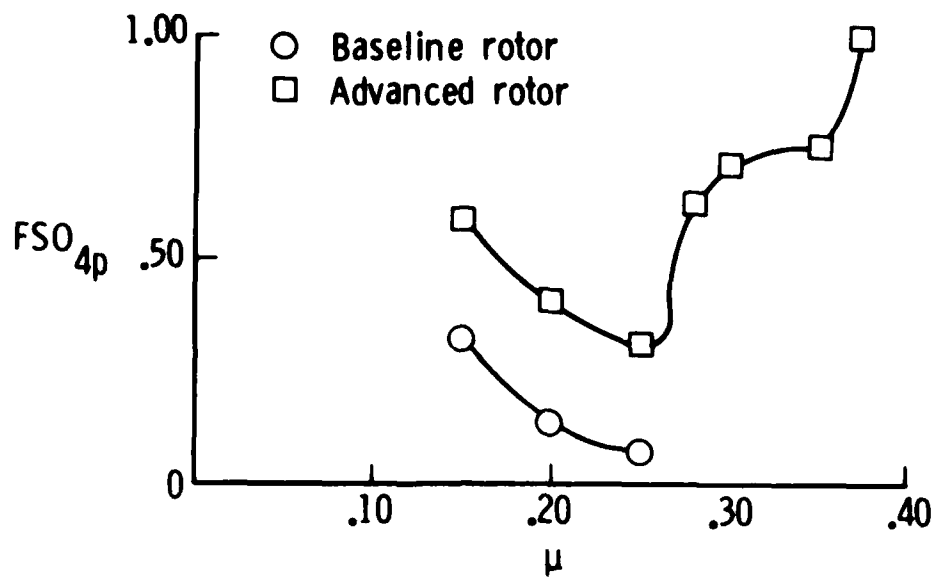
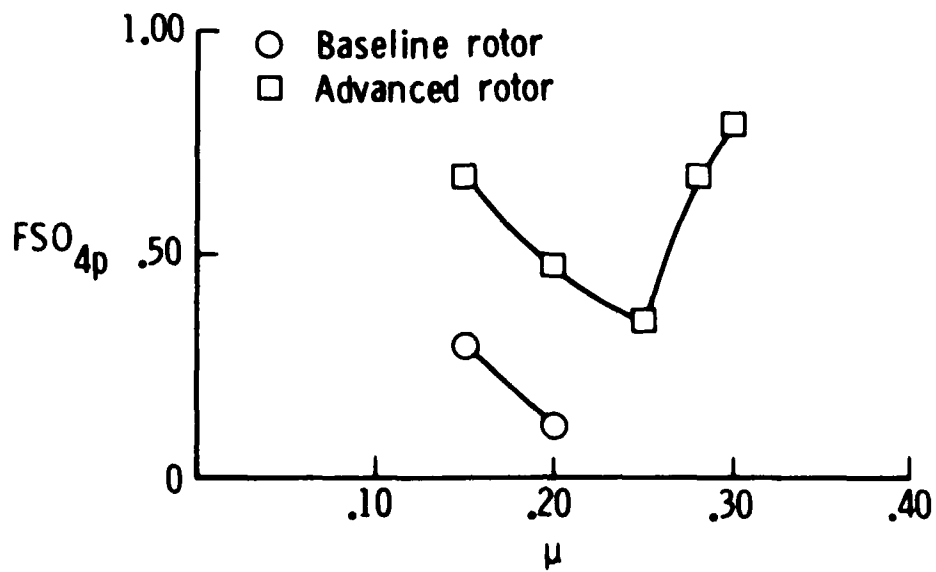(c) Gross weight = 20 500 lb; C_L = 0.00898.

(d) Gross weight = 22 500 lb; C_L = 0.00985.
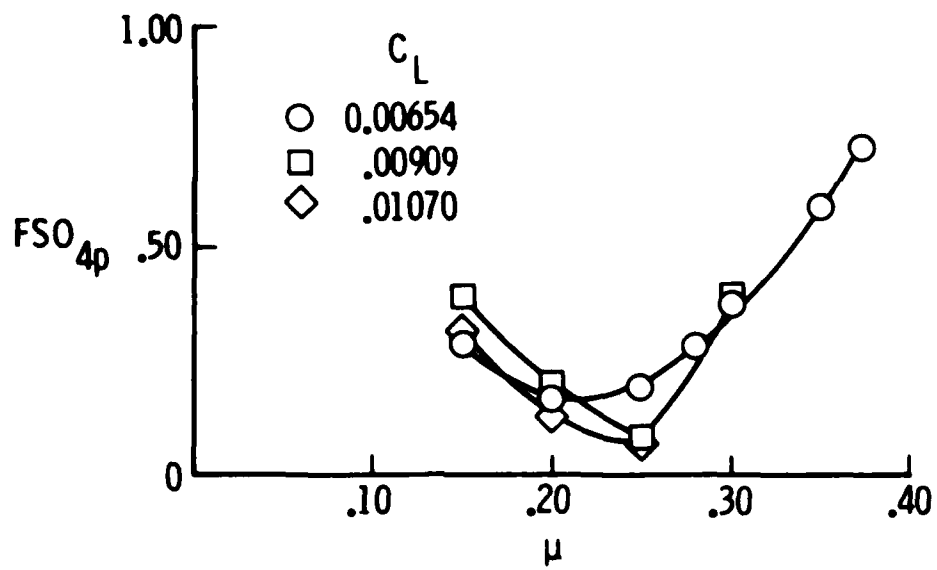
Figure 19. Continued.

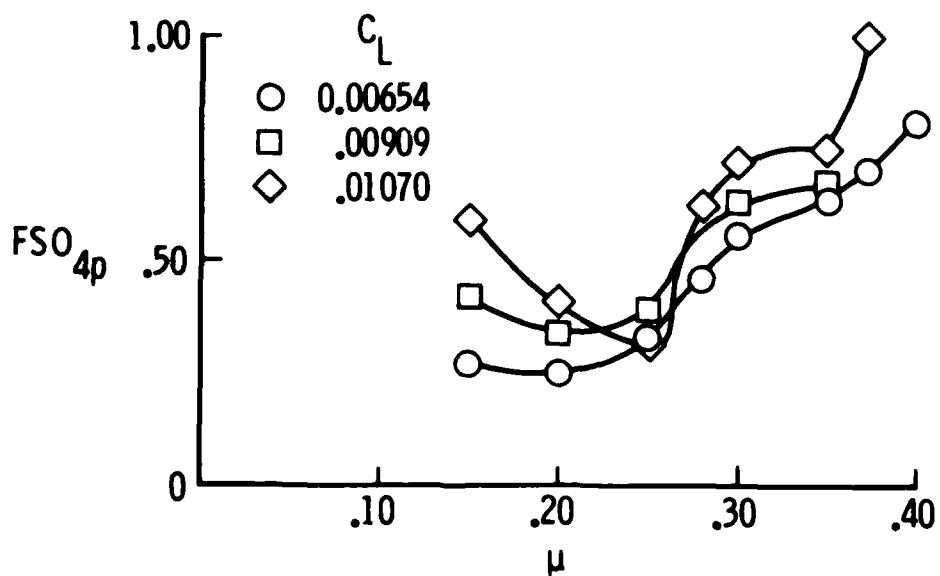(e) Gross weight = 24 500 lb; C_L = 0.0107.

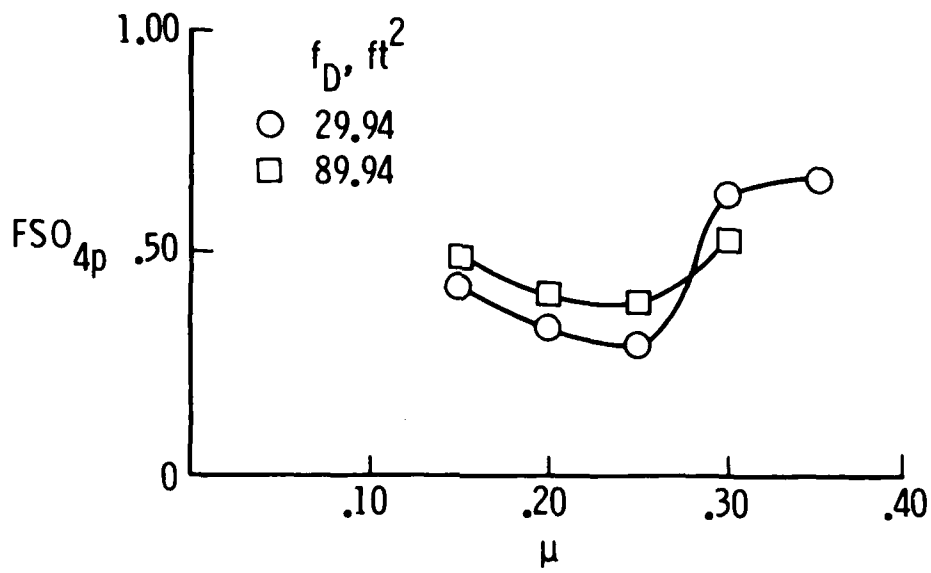(f) Gross weight = 26 500 lb; C_L = 0.0116.

Figure 19. Concluded

(a) Baseline rotor.

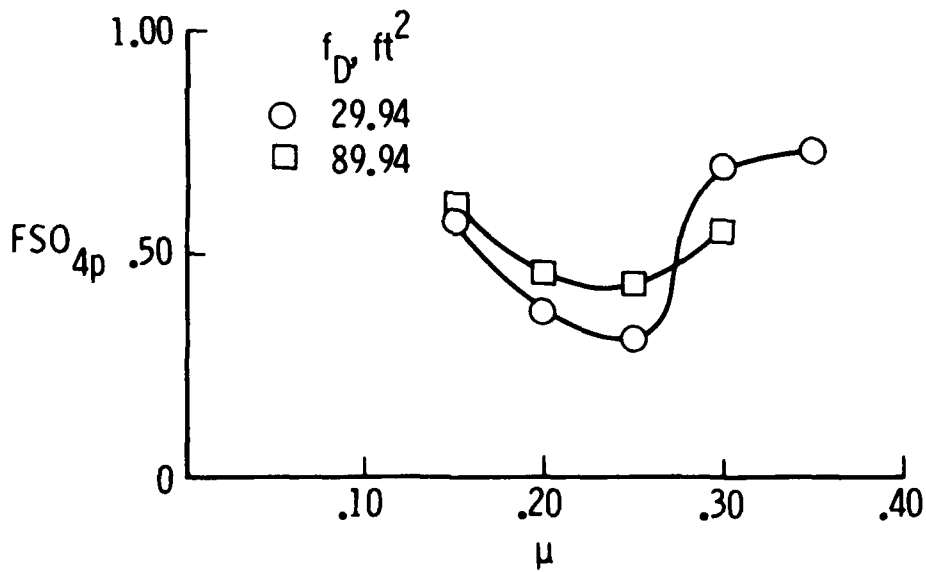(b) Advanced rotor.

Figure 20. Effect of C_L on 4-per-rev fixed-system loads for $f_D = 29.94$ ft^2.

(a) Sea level, 95°F; $C_L = 0.00909$.

(b) 1000 ft, 95 F; $C_L = 0.0105$.

Figure 21.- Effect of vehicle flat-plate drag on advanced rotor 4-per-rev fixed-system loads at a gross weight of 24000 lb.
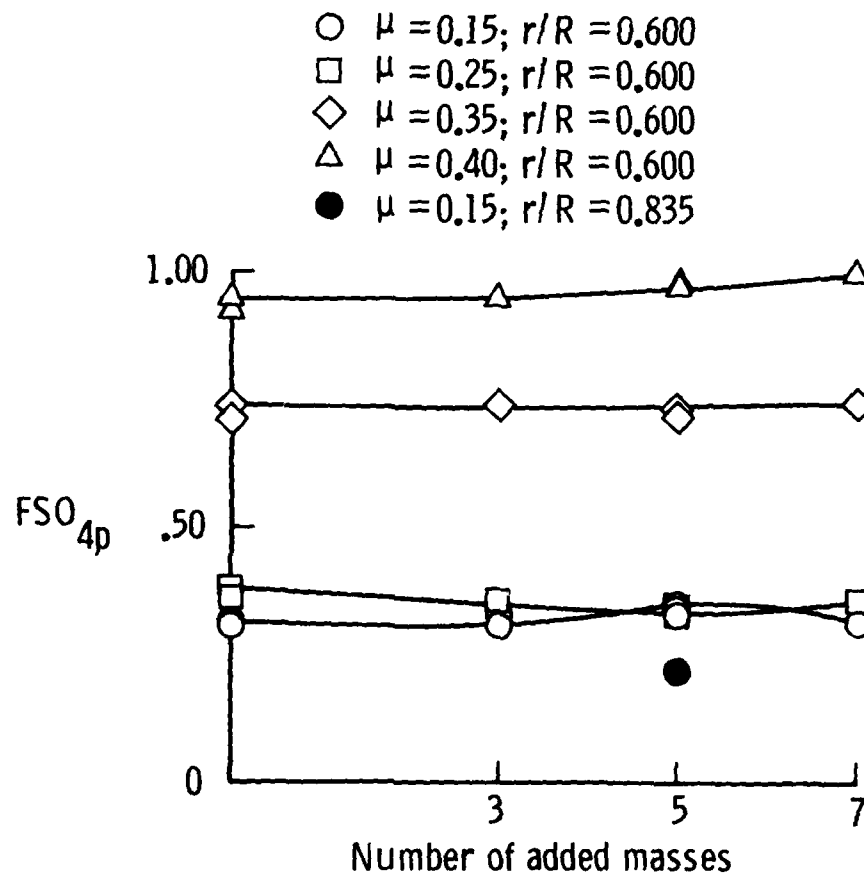
Figure 22. Effect on 4-per-rev fixed-system loads of adding nonstructural mass to advanced rotor for a gross weight of 18500 lb ($C_L = 0.00654$), SLS, and $f_D = 29.94$ ft^2.

A/84 514

NASA

National Aeronautics and
Space Administration

Report Documentation Page

1. Report No. NASA TM-89129 AVSCOM TM-87-B-8	2. Government Accession No.	3. Recipient's Catalog No.
4. Title and Subtitle Wind-Tunnel Evaluation of an Advanced Main-Rotor Blade Design for a Utility-Class Helicopter		5. Report Date September 1987
		6. Performing Organization Code
7. Author(s) William T. Yeager, Jr., Wayne R. Mantay, Matthew L. Wilbur, Robert G. Cramer, Jr., and Jeffrey D. Singleton		8. Performing Organization Report No. L-16260
9. Performing Organization Name and Address Aerostructures Directorate USAARTA-AVSCOM NASA Langley Research Center Hampton, VA 23665-5225		10. Work Unit No. 505-61-51-03
		11. Contract or Grant No.
12. Sponsoring Agency Name and Address National Aeronautics and Space Administration Washington, DC 20546-0001 and U.S. Army Aviation Systems Command St. Louis, MO 63120-1798		13. Type of Report and Period Covered Technical Memorandum
		14. Army Project No. 1L162209AH76B

15. Supplementary Notes

William T. Yeager, Wayne R. Mantay, Matthew L. Wilbur, Robert G. Cramer, Jr.,
and Jeffrey D. Singleton: Aerostructures Directorate, USAARTA-AVSCOM.

16. Abstract

An investigation was conducted in the Langley Transonic Dynamics Tunnel to evaluate differences
between an existing utility-class main-rotor blade and an advanced-design main-rotor blade. The two
rotor-blade designs were compared with regard to rotor performance, oscillatory pitch-link loads, and
4-per-rev vertical fixed-system loads. Tests were conducted in hover and over a range of simulated
full-scale gross weights and density altitude conditions at advance ratios from 0.15 to 0.40. Results
indicate that the advanced-blade design offers performance improvements over the baseline blade in
both hover and forward flight. Pitch-link oscillatory loads for the baseline rotor were more sensitive
to the test condition than those of the advanced rotor. The 4-per-rev vertical fixed-system load
produced by the advanced blade was larger than that produced by the baseline blade at all test
conditions.

17. Key Words (Suggested by Authors(s)) Helicopters Model rotor testing Helicopter rotor performance Blade loads	18. Distribution Statement Unclassified Unlimited Subject Category 02		
19. Security Classif.(of this report) Unclassified	20. Security Classif.(of this page) Unclassified	21. No. of Pages 37	22. Price A03

END

10-87

DTIC